ALTERNATIVE DESIGN CONCEPTS FOR THE ELECTRON TO PHOTON CONVERTER IN THE ACCELERATOR BASED PRODUCTION OF TECHNETIUM-99M

BY

JESS L. IVERSON

B.SC., NUCLEAR ENGINEERING (1995)
UNIVERSITY OF ARIZONA

SUBMITTED TO THE DEPARTMENT OF NUCLEAR ENGINEERING
IN PARTIAL FULFILLMENT OF REQUIREMENTS FOR THE DEGREE OF

MASTER OF SCIENCE IN NUCLEAR ENGINEERING

AT THE

MASSACHUSETTS INSTITUTE OF TECHNOLOGY

AUGUST 1997

SIGNATURE OF AUTHOR.....
DEPARTMENT OF NUCLEAR ENGINEERING
AUGUST 20, 1997

CERTIFIED BY.....
PROFESSOR LAWRENCE M. LIDSKY
THESIS SUPERVISOR

READ BY.....
DR. RICHARD C. LANZA
THESIS READER

ACCEPTED BY.....
JEFFREY FREIDBERG
CHAIRMAN, DEPARTMENTAL COMMITTEE ON GRADUATE STUDENTS

ALTERNATIVE DESIGN CONCEPTS FOR THE ELECTRON TO PHOTON CONVERTER IN THE ACCELERATOR BASED PRODUCTION OF TECHNETIUM-99M

BY

JESS L. IVERSON

SUBMITTED TO THE DEPARTMENT OF NUCLEAR ENGINEERING
ON AUGUST 20, 1997, IN PARTIAL FULFILLMENT OF THE
REQUIREMENTS FOR THE DEGREE OF
MASTER OF SCIENCE IN NUCLEAR ENGINEERING

ABSTRACT

The photonuclear production of radioisotopes using electron LINAC bremsstrahlung sources offers an industry alternative to reactor and ion beam production methods. One such method under development is the utilization of the Giant Dipole Resonance in the (γ,n) reaction cross-section. This method is being studied for use in the production of ^{99m}Tc from enriched ^{100}Mo by electron beam induced bremsstrahlung photons. Of primary concern to any radioisotope production system is the specific activity it is able to create of the radioisotope. In a photoneutronic production system maximizing the number of GDR photons on a given target increases the specific activity. Proper design and optimization of the electron-to-photon converter maximizes the number of GDR photons. This study examines some alternative types of converter design. MCNP is used to predict isotope yields and energy deposition in the converter assemblies and an Excel Spreadsheet is used to analyze the heat-transfer capabilities of the systems. Optimized designs are presented for the different types of converters studied. A radiantly cooled converter is presented as a low-yield design, while a circulating loop of molten lead is analyzed for use in a high-yield system.

Thesis Supervisor: Lawrence M. Lidsky
Title: Professor of Nuclear Engineering

Thesis Reader: Richard C. Lanza
Title: Senior Research Scientist

ACKNOWLEDGEMENTS

I would like to thank my wife, Terri, for all of her love and understanding during the time I have been working on my thesis. Without her support I'm quite sure that this would not have been finished. I know that I have been hard to live with at times. Thanks for putting up with me. The computer is yours anytime you want to use it.

I would also like to thank Professor Lidsky and Dr. Lanza for their help and patience during this time. I realize that things have been rushed here at the end and for that I would like to apologize. Thanks for helping me to complete this document.

Thanks also go to my brother Erik for his many words of encouragement and his late night proof-reading. Without which I'm not sure where I'd be.

Finally, I would like to thank my Father and late Mother. For it is all of their love and encouragement that was able to get me here in the first place.

Jess Iverson

TABLE OF CONTENTS

LIST OF FIGURES

List of Tables

1. INTRODUCTION

Every year, radioisotopes (radioactive isotopes) are used in millions of industrial, scientific, and medical applications[10]. These uses range from tracking the dispersion of chemicals in the water aquifer to identifying tumors in cancer patients. In many cases there simply is no other way to gather the information gained from radioisotope testing. For this reason a constant, reliable source of high-grade radioisotopes is of utmost importance.

One of the most important uses of radioisotopes is in the field of medical testing. One in three hospitalized patients undergo some type of test or treatment involving nuclear medicine. Radioisotopes are used in almost 36,000 imagining procedures and 29,000 laboratory tests every day in the United States alone. Over 80% of these tests utilize ^{99m}Tc[3]. When combined with a variety of pharmaceutical carriers, ^{99m}Tc can be used to study nearly every major system in the human body. For instance, ^{99m}Tc pertechnetate is used to study the thyroid and salivary glands, while ^{99m}Tc exametazine is used to study the brain. It is even possible to tag red blood cells with ^{99m}Tc to study gastrointestinal bleeding and the chambers of the heart.

^{99m}Tc has a half-life of 6.03 hours. Normally, this would make a radioisotope very difficult to transport for use anywhere other than at its production facility. However, ^{99m}Tc is actually the daughter product of ^{99}Mo. The ^{99}Mo decays with a half-life of 66 hours to the ^{99m}Tc. This gives a relatively large time frame for the molybdenum-technetium mixture to be transported for use. Typically the mixture is packaged in football sized "generators". Contained in the generators are chromatographic columns in which the ^{99}Mo is stored. Once on-site the ^{99m}Tc is separated from the ^{99}Mo by passing a

saline solution over the chromatographic column which is then mixed with the appropriate pharmaceutical carriers. The ^{99m}Tc decays primarily (89.1%) by emitting a low energy (140.5 keV) gamma ray. This decay scheme results in delivering a fairly low dose to the patient, while still having a sufficient energy and reasonable time frame for detection outside of the body.

Most commercial radioisotopes are produced either by nuclear reactors or by heavy particle accelerators[8]. By far, the majority of radioisotopes are produced by fission product separation from highly enriched uranium (HEU) targets placed in nuclear reactors. This separation process is extremely difficult and expensive. Complex remote handling facilities must be used to safely extract the various useful isotopes from the highly radioactive HEU targets. The majority of the processing uses a variety of chemical reactions to separate the different isotopes from one another; this generates a large volume of chemically and radiologically dangerous waste.

However, there are also a number of advantages to producing radioactive isotopes, including ^{99}Mo, in nuclear reactor cores. Originally, ^{99}Mo was produced commercially by neutron absorption in natural molybdenum or enriched ^{98}Mo. The disadvantage of this type of production was that it led to fairly low specific activities for the ^{99}Mo, in the several Curie/gram range. Therefore, in order for the saline solution to extract reasonable amounts of ^{99m}Tc, the generators shipped to the hospitals were quite large. These larger generators required a significant amount of shielding, which made them difficult to transport from the production facility to the end-user. On the other hand reactor produced fission product ^{99}Mo has activities on the order of 10^4 Curie/gram. In some cases it was actually necessary to dilute the ^{99}Mo since the excessive radiation

would damage the chromatographic columns it was being transported in. This high activity allowed the generators to become very compact. With shielding the generator is approximately the size of a football.

Currently, ^{99}Mo production is reaching a crisis point in North America. The only facility producing ^{99}Mo in useful quantities is the near 40-year-old NRU reactor in Chalk River, Ontario. The reactor is scheduled to be shutdown in the year 2000 and recently labor problems and aging equipment at the plant have caused numerous unexpected temporary shutdowns. The NRU reactor is scheduled to be replaced by the Maple-10 isotope reactors in Canada. There are also plans for the conversion of an existing Department of Energy reactor to the production of ^{99}Mo at Oak Ridge National Laboratory. However, there are no guarantees as to when and if these replacement reactors will reach production capacity. Assuming they are replaced, the new reactors will continue to use HEU targets, and therefore the problem of dealing with high-activity fission product waste will persist. This situation is obviously unstable, and it is readily apparent that multiple sources of such an important medical resource are necessary.

1.1 PHOTO-PRODUCTION OF ^{99M}TC

Currently research is being done on the use of electron beams in the production of radioisotopes. The reaction of interest explored in this study is the photoneutronic (γ,n) reaction in ^{100}Mo initiated by electron beam induced bremsstrahlung. This reaction results in the production of ^{99}Mo, the parent of ^{99m}Tc. Over most of the energy spectrum the cross-section for this reaction is very low, but there is a resonance in the photon absorption cross-section, known as the giant dipole resonance (GDR), which occurs between 8 MeV and 20 MeV for ^{100}Mo. Figure 1 below shows the cross-section of the GDR for ^{100}Mo over its energy range.

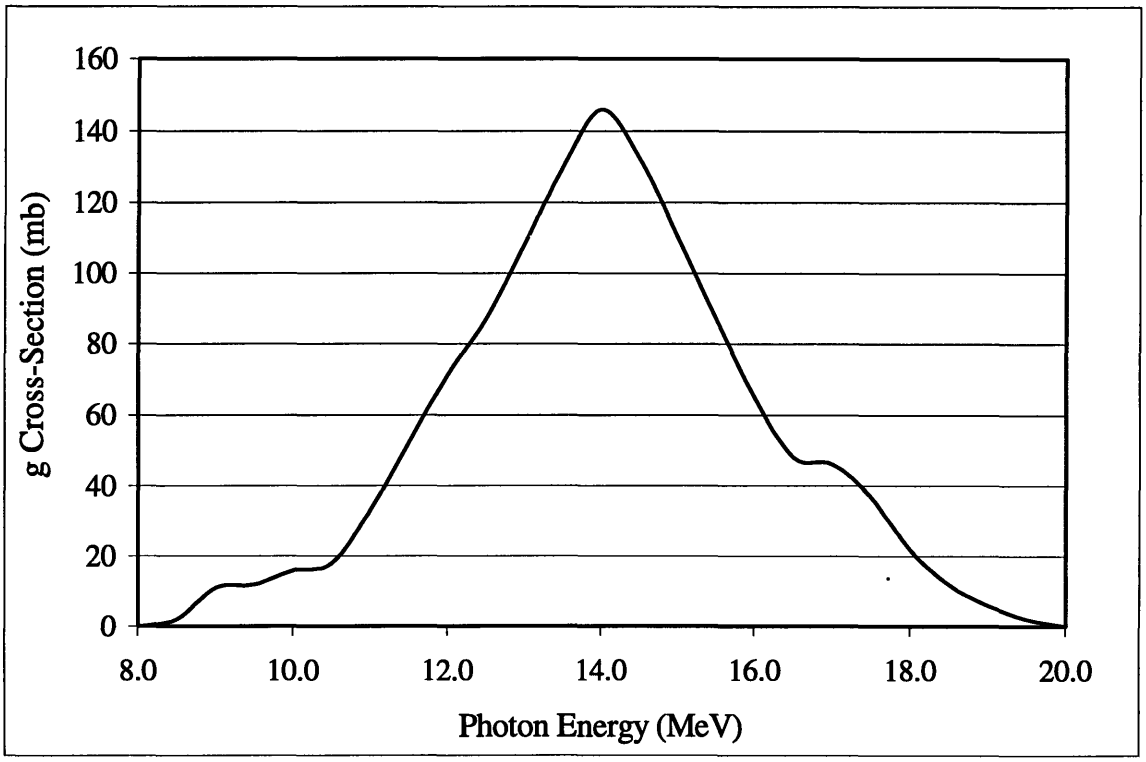

FIGURE 1: GIANT DIPOLE RESONANCE FOR MOLYBDENUM-100

If a photon beam is concentrated in this energy region it is possible to achieve very high reaction rates, subsequently creating high specific activities of ^{99}Mo. The utilization of this type of reaction is not limited to the production of ^{99}Mo. The giant dipole resonance

is a result of the forces caused by the interaction of photons and neutrons in the atomic nucleus, and therefore exists in some capacity for all isotopes. The peak energy of the resonance roughly decreases as the atomic mass of the nuclei in question increases. The full width at half-maximum of the peak remains fairly constant for any resonance, while the total area of the resonance increases with atomic mass. Therefore, this type of reaction is much easier to take advantage of with heavier elements.

The difficulty in using this production technique for other isotopes is not so much a problem in nuclear science as it is in chemistry. Since the technique produces fairly low specific activities, the daughter nuclei must be easily separable from the parent nuclei. This is true in the case of ^{99m}Tc. The enriched ^{100}Mo target is exposed to the photon beam and a portion of it is transformed to ^{99}Mo. Technetium and molybdenum are then easily separated, either in an ion exchange column or in a thermal sublimation system. Therefore, as the ^{99}Mo decays to ^{99m}Tc it is easily removed. After economically optimal amounts of the radioisotope have been used, the unconverted enriched ^{100}Mo is returned to the production facility to be recycled. For this type of system to be useful in the production of other radioisotopes a similar separation scheme must be available.

The photon beam used for this reaction is provided by the conversion of high energy accelerated electrons to bremsstrahlung photons in a high-Z material, such as tungsten or lead. The high-Z material portion of the system is referred to as the converter, since it converts electrons into photons. The electron beam is generated using a LINAC. Typical LINACs are capable of operating over a range energies, with the maximum beam current at any energy determined by the power supply and design of the system. The LINAC which this project is based on, manufactured by Thermo Technology

Ventures, is designed to be operated at 450 mA current at a 0.001 duty factor for 50 MeV Electrons, which would provide a average beam power of 24.5 kW. This LINAC can be set to any current below the line, shown in Figure 3 below, for electron energies between 28 MeV and 68 MeV.

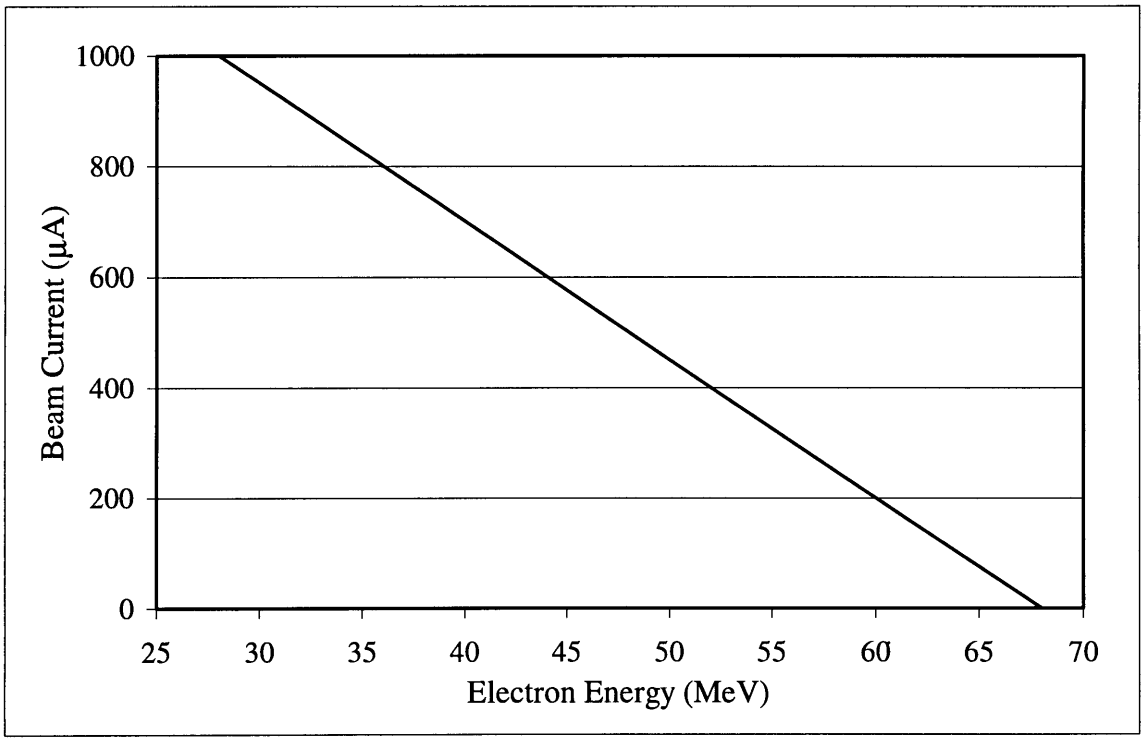

FIGURE 2: MAXIMUM BEAM ENERGY VERSUS MAXIMUM BEAM CURRENT

So while it is possible to use the accelerator to produce 65 MeV electrons, the current would be so low that almost nothing can be done with the beam. A large portion of the electron beam energy will ultimately be deposited in the electron-to-photon converter.

1.2 ELECTRON-PHOTON CONVERTER

The design of the electron-photon converter can have a drastic effect on the efficiency of this type of isotope production system. By increasing the photon beam on a given target the specific activity of the end product can be substantially increased.

However, this also has the effect of increasing the amount of energy deposited in both the converter and target. Therefore, these components must be designed to optimize their heat removal characteristics and to minimize the unnecessary energy deposited in them. The object of this study is to optimize the design of the electron-photon converter and to devise a cooling method to maintain it in operating condition.

2.0 CONVERTER DESIGN STRATEGY

2.1 THEORY

One of the most important design parameter in a radioisotope production system is yield, which is the amount of the original target material converted into the desired isotope. The other is the specific activity, which is the decay rate per unit mass in the target. The yield in a ^{99}Mo photo-production system is determined by two factors. The first factor is the enrichment of the ^{100}Mo in the target assembly. The second factor is the number of photons incident on the target whose energy is within the range of the Giant Dipole Resonance for the (γ,n) reaction in ^{100}Mo. In turn, the yield is limited by the rate at which heat is deposited in the converter and target assemblies. The heat deposition rates in these systems can get very high; so high as to melt the tungsten or molybdenum contained in them within a few seconds without cooling.

The photon flux on target is determined by the current of the electron beam and the conversion rate of electrons to bremsstrahlung photons in the converter. The energy of the electron beam and the attenuation characteristics of the converter and target determine the photon spectrum, and therefore the number of photons that fall within the Giant Dipole Resonance region. Clearly the goal is to maximize the flux on target of photons in the energy range of the Giant Dipole Resonance. This is achieved by using a high-Z material for the electron-photon converter. However, high-Z materials are also quite efficient at absorbing photons, so the design must be such as to minimize the shielding effects. The optimal thickness for photon production is approximately half the electron range in the material, so that a residual electron beam is mixed with the photon beam at the converter plate exit. Finally, the distance from the converter to the target

must be minimized. The electron beam produced by the accelerator is essentially mono-directional. However, the photons generated in the converter are not, although the high-energy photons of interest are primarily forward scattered. Therefore, it is important to minimize the distance between the converter and target while still leaving room to remove the residual electron beam by magnetic deflection or absorption in a material relatively transparent to GDR photons.

In addition to the optimizing the conversion rate of electrons to GDR photons, the flux on target may also be improved by increasing the current of the electron beam. However, this has the effect of increasing the amount of heat deposited in the electron-photon converter and the molybdenum target. Therefore, the current may only be raised to a certain level. This level is set by the maximum heat removal characteristics of the converter and target systems.

Therefore, the system is optimized by designing it in such a way as to maximize the conversion of electrons into photons in the Giant Dipole Resonance energy range and its heat transfer characteristics. The beam current may then be increased until the cooling system reaches its upper limitations. A series of analysis were performed with a variety of converter designs to observe trends in system performance. These trends were then used to determine system design parameters. Finally, consideration was taken for the complexity of the system in both use and construction. For a production facility to be successful it needs to be reliable and simple to use.

2.2 Types of Converter Designs to be Considered

The baseline design for the converter system is a 1-cm long slug of porous tungsten, equivalent to a 0.35-cm long slug of nonporous tungsten. Forcing helium through the pores in the metal cools the slug of tungsten. This is known as a porous metal heat exchanger (PMHX). This system performs quite well at low to moderate beam currents and is well proven with years of experimentation to back it. However, it is incapable of cooling a system at high beam current unless the helium is at an elevated pressure and flow rate. This would require the use of a complex pumping system for a gas-to-gas or gas-to-water heat exchanger.

The main theories behind the following conceptual designs are not only the maximization of heat transfer and GDR photon flux on target, but also the simplification of system design. Simple designs typically translate into higher capacity factors and system efficiency. For this reason a great deal of effort has gone into engineering electron-to-photon converter designs that have no moving parts. Two overall design concepts were chosen for this study. The first design was chosen for its simplicity, the second for its ability to handle very high heat loading.

2.2.1 RADIANTLY COOLED CONVERTER

A radiantly cooled converter is very attractive for the simple fact that it has no moving parts. Since tungsten's melting point is at 3660K the converter is able to operate at a very high temperature (2500K→3000K), which allows the radiant heat transfer to become very efficient. The primary disadvantage of the radiantly cooled system is the amount of surface area on the converter required for adequate head transfer to take place. By using the basic laws of radiant heat transfer, a conservative model of the system can be generated. This simple model is based on the assumption that the heat deposition is uniform across the entire slab. In the actual system the heat is deposited only in the path of the beam, which appears as an elongated oval over the length of the slab. Therefore, the area calculated by this model is of the center oval and not the entire slab. The rest of the slab acts as a heat sink, but is not considered here to improve the model conservatism. The conduction of heat from the beam path to the heat sink causes the actual peak temperature on the slab to be substantially lower (100K→150K) than the one generated by this simple model. The basic equation governing the simple radiant heat transfer model is as follows:

$$q = \varepsilon \cdot \sigma \cdot A \cdot \left(T_{sur}^4 - T_s^4\right)$$

Where ε = Emissivity of Surface (average for Tungsten = .225)
σ = Stephan-Boltzman Constant (5.67E-12 W/cm^2K^4)
A = Surface Area of object (cm^2)
T_{sur} = Temperature of Radiant Surface (K)
T_s = Temperature of Surrounding (K)

A typical target in this system will have to be able to reject 2000 to 5000 watts of power, or an average of about 3500 watts. Therefore, at a surface temperature of 3000K and a surrounding temperature of 300K, the surface area would have to be approximately 34

cm^2 in order to reject 3500 watts of power. Figure 4 below shows a comparison of the required surface areas for different values of heat deposition. The top line represents the requirements for a surface temperature of 2500K and the bottom for 3000K.

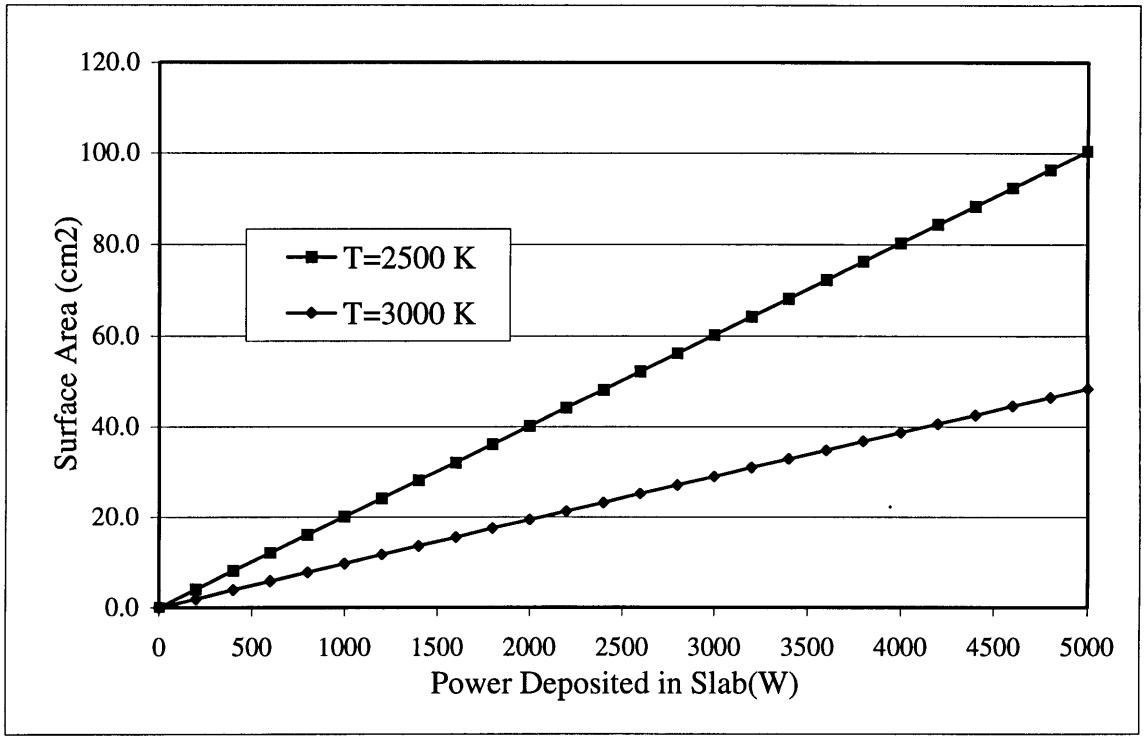

FIGURE 3: SURFACE AREA REQUIREMENTS FOR RADIANT HEAT TRANSFER

For this reason the design of a radiantly cooled target must be centered on maximizing the surface area available for heat transfer. Three different designs were considered for the radiantly cooled target. The first design is a singular plate of tungsten placed at a very shallow angle in the beam bath. By having the beam strike the plate of tungsten at a shallow angle the area over which the beams energy is deposited is greatly increased. This has the negative effect of increasing the length and thereby placing the converter at an average distance further from the converter, lowering the flux on target. The second design considered was that of multiple plates of tungsten set at opposite angles to one another. This was chosen because it would increase the surface area of the converter and

it would make the average distance from converter to target more uniform over the beam cross-section, thereby leveling the flux-distribution over the surface of the molybdenum target. Finally, a cone shaped model was analyzed. This design was chosen because by facing the cone in the direction of the beam the point of the cone is placed nearest the target. Therefore, the small scattering angle, high-energy photons that are generated in the point have a much higher probability of striking the molybdenum target.

2.2.2 Molten Lead Converter

A molten lead target was considered for analysis when the heat deposition limitations of the radiant cooled converter were reached. A molten lead converter has a number of advantages over the solid tungsten converter, primarily that since the lead is already a liquid there is no need to worry about melting it. The lead is simply pumped in a small circulating loop with a lead-to-water heat exchanger. At one point in the loop the flow is pinched and the walls of the tubing narrowed where the beam will strike. The heat exchanger is scaled so as to allow adequate heat transfer for the amount of deposited energy. This makes the lead loop substantially easier to cool than the tungsten target. If greater cooling of the lead is required the size of the heat exchanger can be increased to allow for additional heat transfer. Another significant advantage to a lead converter is that it has a better conversion rate of electrons to GDR photons than does tungsten. The disadvantage, compared to the radiantly cooled tungsten target, is that a liquid system is more complex, requiring a pump and heat exchanger. However, if the design uses an electromagnetic force pump then there are no moving parts in the cooling loop. Electromagnetic force pumps have been proven to work quite well with liquid lead systems. By eliminating all moving parts in the system, the opportunities for system

failure are significantly decreased. Preliminary analysis of the molten lead converter showed a number of advantages over either the PMHX cooled slug or the radiantly cooled slab and it was therefore chosen for the most detailed study, including the design of an operational system.

2.3 Computer Modeling

Two different phases of computer modeling were performed for this project, nuclear interaction and heat transfer. For the radiantly cooled model the capacity of the design was so tightly linked to the heat transfer characteristics that the models were performed in parallel so as to asses the viability of various perturbations before extensive research time was spent on them. For the molten lead converter the nuclear interaction analysis and heat transfer analysis were performed separately. This is acceptable since it is possible to simply scale the heat transfer system to the requirements of the loop design. The computer analysis was performed on a Pentium-200MMX processor based personal computer.

2.3.1 Electron-Photon Transport

The electron and photon modeling was performed using MCNP (Monte-Carlo N-Particle) version 4A. MCNP is a time-dependant, continuous energy, coupled neutron/photon/electron Monte Carlo transport code. By defining a geometric system, and all materials contained within it, it is possible to model most types of electron, photon, and neutron interactions. If the tallying system in MCNP is used properly, it is capable of providing very accurate models of electron and photon transport in the converter/target systems. MCNP is not capable, without modifications, of modeling (γ,n)

reactions, because it does not contain the requisite cross-sections. Cross-section data is available in the physics literature, although it is somewhat difficult to correct for (γ,pn) reactions. The following MCNP tally card can model the photoneutronic reaction rate due to the (γ,n) and (γ,np) reactions in a molybdenum target cell:

```
F4:P 1
c If cell 1 is the molybdenum target then Tally Type 4 calculates the photon flux averaged over the
c target
E4 8 8.5 9 9.5 10 10.5 11 11.5 12 12.5 13 13.5 14 14.5 15 15.5 16 16.5 17 17.5 18 18.5 19 19.5 20
c The E card divides Tally 4 into the specified energy bins from 8 to 20 MeV
EM4 0 2 11 12 16 18 33 52 71 87 108 130 146 132 110 87 65 48 46 37 22 12 6 2 0
c The EM card multiplies each of the energy bins by the indicated value, in this case the cross-
c section for (γ,n) and (γ,np) reactions in 100Mo in the respective energy bin
```

FIGURE 4: MCNP TALLY CARD FOR DETERMINING MOLYBDENUM YIELD

A tally type 4 generates the average flux of the specified particle type, in this case photons, over the entire volume of the designated cell per input electron. The E card divides the tally so that the photon flux in each energy range is determined, i.e., the flux with energies from 8 to 8.5 MeV, 8.5 to 9 MeV, etc. Each of the energy specific fluxes is then multiplied by the cross-section for ^{100}Mo in that energy range. Since flux multiplied by a cross-section equals the reaction rate, this card can compute the rate at which ^{99}Mo is produced in the target slug. This tally's results have been verified by experimental research carried out at the Rensselaer Polytechnic Institute. In this experiment molybdenum foils were irradiated in a 40 MeV electron LINAC and the induced activities were within 5% of the values predicted by this tally.

At this point it becomes necessary to define several figures of merit that will be used to compare the various models during this study.

Yield: This refers to the flux of GDR photons averaged over the molybdenum slug multiplied by the molybdenum (γ,n) reaction cross-sections listed above, thus

giving an averaged (γ,n) reaction rate over the molybdenum slug. It should be noted that the flux of photons is relative to the flux of incident particles, i.e., it is a percentage of the incident number of electrons.

Current-Weighted Yield: This is simply the yield multiplied by the ratio of the relevant current for the electron beam to the current of the slug baseline model (250μA). This value will help to show the difference between various designs in regards to the beam current at which they can be operated.

Analyzing several tallies produced by MCNP will generate these values. Sensitivity studies will then be performed to determine optimum designs.

2.3.2 Heat Transfer Model

Two spreadsheet-based heat transfer models were used for the analysis of the converter designs, one for the radiantly cooled converter and one for the molten lead converter. Both of these spreadsheets are shown in Appendix B. A spreadsheet-based model was chosen over the use of a complex heat transfer code for its ease of use. While the use of a commercial heat transfer code, such as ALGOR or HEATING, may have given a more detailed analysis, it was determined that this simply wasn't needed for the goals of the project. A conservative estimate model would accurately predict whether or not a given system is capable of functioning at operational conditions without destroying itself. As long as all errors are on the side of conservatism, then a more detailed model would only show that the system works even better than predicted.

The radiant heat transfer spreadsheet is based on an iterative step approach to modeling heat transfer in the system. The slab of tungsten is first divided into four symmetrical pieces. One of the quadrants is then broken into a grid of individual cells

that is 30 cells wide and 50 cells long, thus making each individual cell a very small portion of the slab. Now consider one cell within the grid. The initial temperature of the cell is set to 3000 K, the approximate operating temperature of the tungsten slab. Then the change in the temperature of this cell, due to deposited heat from the electron beam and various heat transfer modes, is determined. This change is then applied to the initial temperature for the next iterative step, or:

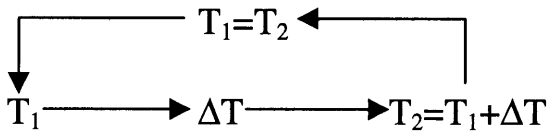

While this method is primarily for modeling transient heat transfer, it is also quite useful in modeling combined mode heat transfer problems when the system can be treated as essentially two dimensional. The problem with combined mode heat transfer problems is that many times it is almost impossible to analytically solve for the governing equations of the entire system. This is readily apparent when the radiantly cooled slab system is considered. The heat deposition of the beam causes a very large temperature gradient over the surface of the slab. Therefore the radiant heat transfer occurs at very different rates over the entire surface. This system is very difficult to solve implicitly, but is relatively simple when the numerical approach is taken. Since the slab of tungsten is so thin, the temperature gradient over the thickness is negligible. Therefore, it can be modeled as two-dimensional system.

As stated the primary equation in such a system is:

$$T_2 = T_1 + \Delta T$$

Where T_1=the cell's initial temperature
ΔT=the temperature rise due to heat transfer
T_2=the cell's temperature after ΔT

To determine the temperature rise in a cell the following equation was used:

$$\Delta T = \frac{Q}{C_P \cdot \rho \cdot V}$$

Where Q=the heat transfer into the cell (J)
C_P=the specific heat of Tungsten
ρ=the density of Tungsten (19.3 g/cm^3)
V=the volume of the cell (cm^3)

The heat transfer into the cell is then determined by summing the power deposition, conduction to/from adjacent cells, and the radiant heat transfer:

$$Q = (q_{BEAM} + q_{COND} - q_{RAD}) \cdot Tstep$$

Where q_{beam}= Power deposited by the beam (W)
q_{cond}= Power transferred to cell by conduction (W)
q_{rad}= Power dissipated by cell by radiation (W)
Tstep= the time step taken by the spreadsheet (s)

The heat transferred to and from the cell by conduction with the cells surrounding it is determined by the following equation:

$$q_{COND} = k \cdot \left(\frac{dx \cdot dz \cdot (T_1 - T_C)}{dy} + \frac{dy \cdot dz \cdot (T_2 - T_C)}{dx} + \frac{dx \cdot dz \cdot (T_3 - T_C)}{dy} + \frac{dy \cdot dz \cdot (T_4 - T_C)}{dx} \right)$$

Where k=conductivity of Tungsten (w/cmK)
dx, dy, dz=respective dimensions of the cell (cm)
T_1, T_2, T_3, T_4=temperatures of adjacent cells (K)
T_C=temperature of cell (K)

The heat dissipated by the cell through radiant heat transfer is calculated by the following equation:

$$q_{RAD} = 2 \cdot \left[\varepsilon \cdot \sigma \cdot dx \cdot dy \cdot \left(T_C^{\,4} - T_{SUR}^{\,4} \right) \right]$$

Where ε=the emissivity of Tungsten
σ=Stephan-Boltzman (5.67E-12 w/cm^{2}K^4)
T_{sur}=time step of the iterations (s)

Finally, three of the parameters shown above are temperature dependent and vary significantly over the temperature range of the tungsten slab. The conductivity, specific heat, and emissivity all have substantially different values over the range of temperatures from 1500 K to 3000 K. A linear approximation is sufficiently accurate for our purposes. Figure 5 below shows these approximations:

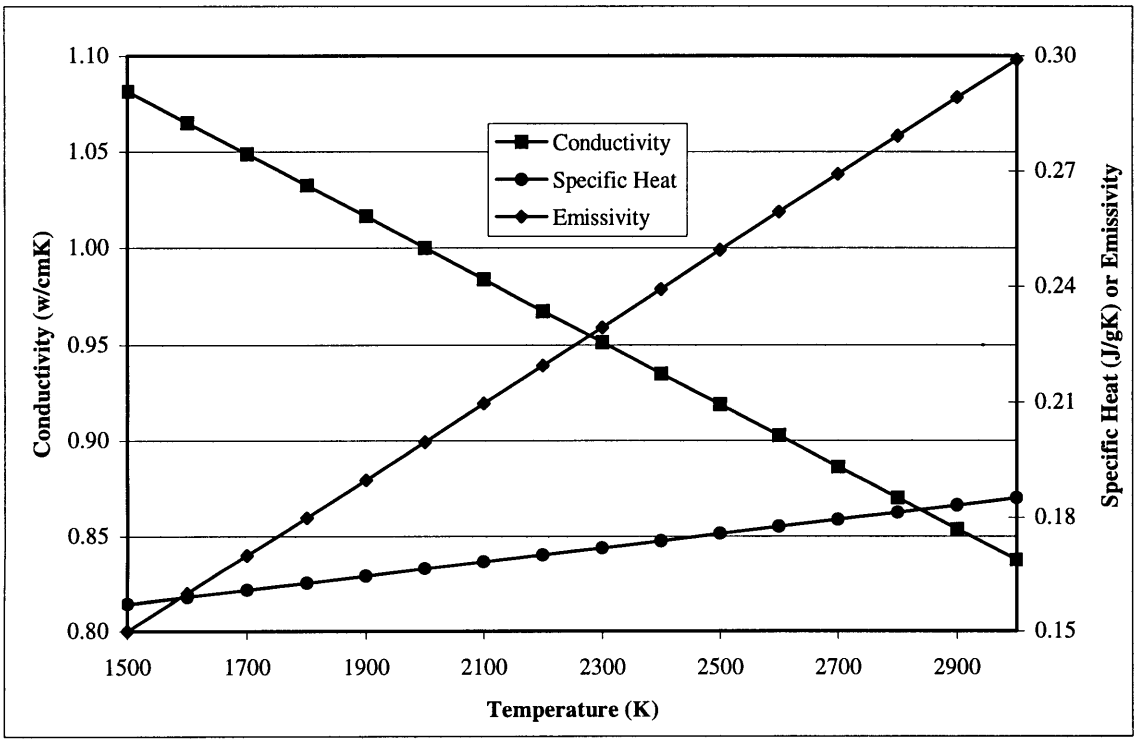

FIGURE 5: TEMPERATURE DEPENDENT PROPERTIES OF TUNGSTEN

In the actual spreadsheet all three of these calculations are actually combined into a single larger equation. Therefore, there are only two values for each cell shown on the spreadsheet, the temperature at the beginning and at the end of the time step.

The spreadsheet model for the molten lead is not as complex as the spreadsheet for the radiantly cooled target. In fact, the only reason a spreadsheet format was used was so that individual parameters could be changed and the results be determined without working through the mathematics by hand every time. This allowed a wide variety of

system parameters to be explored in a relatively short amount of time. The majority of equations used in the spreadsheet are the basic formulas governing conductive and convection heat-transfer.

3.0 PMHX TUNGSTEN SLUG BASELINE CASE

Since the goal of this project is to analyze alternative converter designs, it is necessary to evaluate the initial design. The preliminary design of the converter is based on the use of a 40% porous tungsten slug. The slug is 1 cm in diameter and 0.583 cm long. This corresponds to a thickness of 0.35 cm of solid metal tungsten. Forcing pressurized helium through the porosities from one end of the slug to the other provides heat transfer. The system is operated at a beam energy of 40 MeV and a current of 250 μA, which corresponds to an overall beam power of 10 kW. The molybdenum target will be modeled as a cylinder 1 cm in diameter by 1 cm long and will be placed 5 cm from the end of the converter. The molybdenum target and its placement will be kept consistent for all models to allow accurate comparison of the different designs. The MCNP input deck for the slug converter is given in Appendix A.

The slug converter model has a yield of 2.738±0.033 mb/cm^2. Since the current-weighted yield is defined by the PMHX slug case it also has a value of 2.738±0.033 mb/cm^2. To put these values in more easily understandable terms, a Yield of 2.738 mb/cm^2 corresponds to one ^{100}Mo(γ,n)^{99}Mo reaction for roughly every 7500 incident electrons. Fortunately, a 20 kW beam of 45 MeV electrons is composed of 2.774x10^{15} electrons per second. Therefore, approximately 3.7x10^{11} ^{100}Mo(γ,n)^{99}Mo reactions would occur per second in the molybdenum target. While this reaction rate may at first seem very high, it is in fact quite low when compared to the approximately 4.82x10^{22} atoms of ^{100}Mo in the target slug. It would take 36 hours of irradiation time to convert 0.0001% of the target from ^{100}Mo to ^{99}Mo. The specific activity corresponding to this irradiation time

is 0.3929 Ci/g. Increasing the yield is one of the largest reasons for exploring alternative converter designs. Increasing the yield, by increasing the GDR photon flux on target, is the most direct way of increasing the specific activity of the end product.

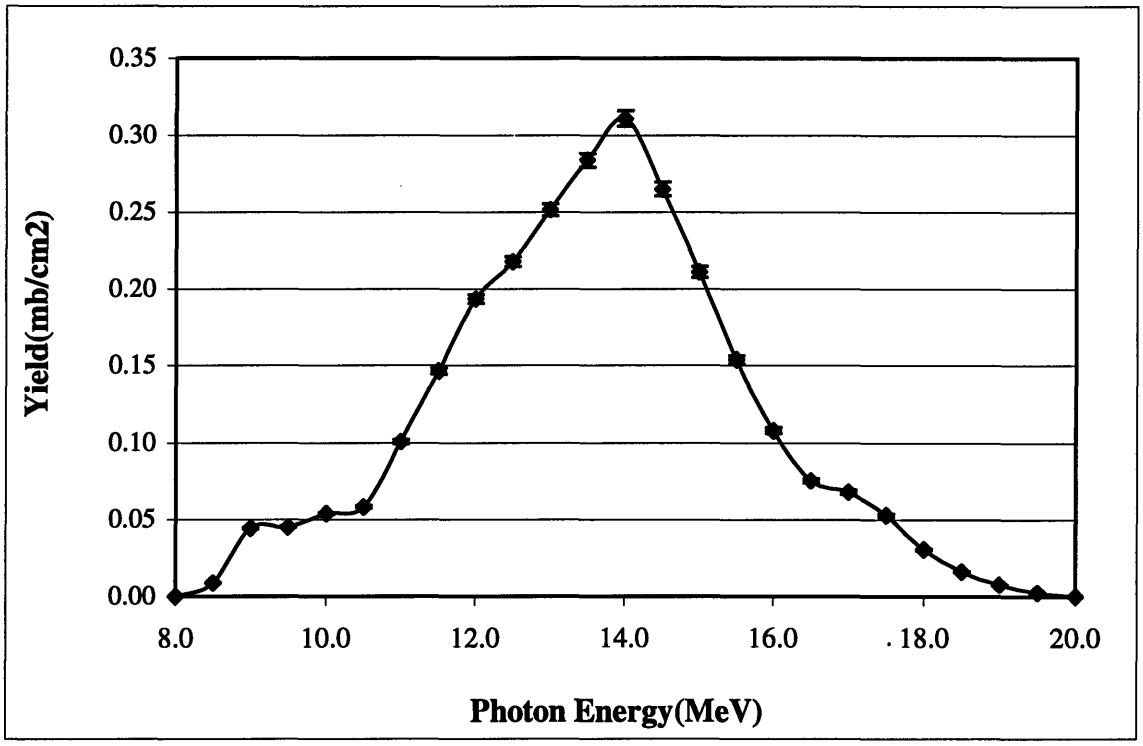

FIGURE 6: YIELD FOR THE PHMX SLUG MODEL

A graph of the yield contribution over the GDR energy range is shown above in Figure 6. As this graph shows, the energy range from 12 to 16 MeV has the most significant contribution to the total yield. At the same time the slug absorbs 14.7 MeV out of every 40 MeV electron. This corresponds to an energy deposition rate of approximately 3.7 kW, or 37% of the total beam power. This provides a baseline for the results from the radiant cooling and lead loop designs to be compared against.

4. RADIANTLY COOLED CONVERTER ANALYSIS

4.1 SINGLE INCLINED PLANE OF TUNGSTEN

The first design chosen for the radiantly cooled converter was a single plane of tungsten placed at a very shallow angle in the electron beam path. The thickness of the tungsten plane is then adjusted so that the electron beam strikes the desired number of grams per square centimeter. By placing the tungsten plane at such a small angle the surface area over which the electron beam strikes the converter is greatly increased. This is illustrated in Figure 7 below.

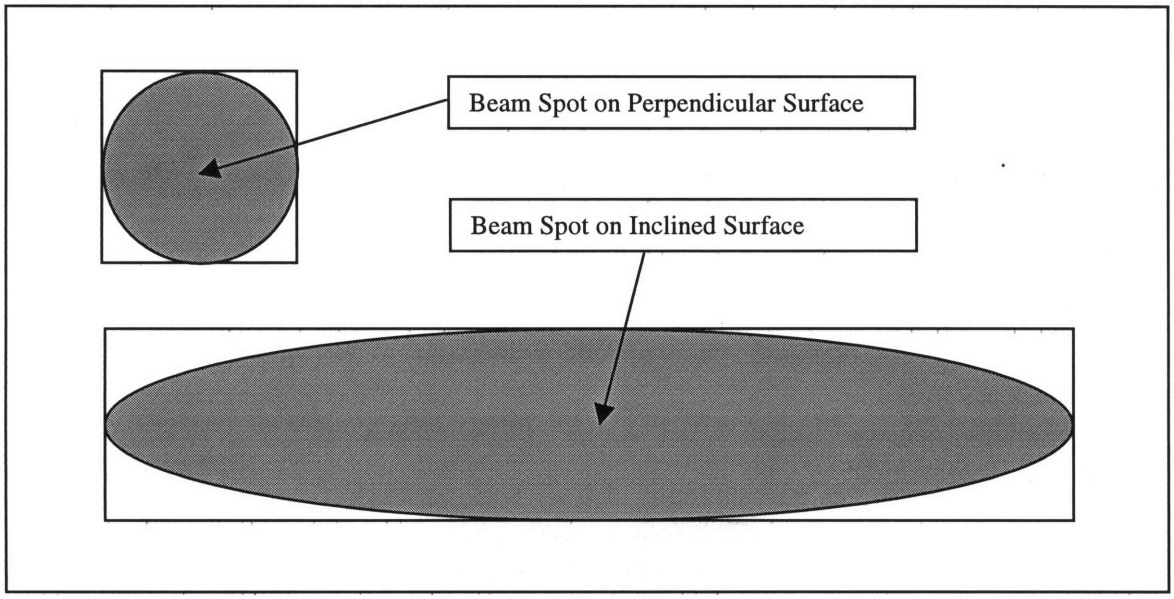

FIGURE 7: RADIANT HEAT TRANSFER FROM INCLINED SURFACE

This increased surface area makes it possible to cool the target by radiant heat transfer alone. A single plane was chosen for preliminary study over other radiantly cooled designs because it does not suffer from the negative effects of a "viewing angle" for radiant heat transfer. In basic radiant heat transfer it is assumed that heat is being radiated from a small surface area to an infinite surface area in all directions. This approximation works quite well as long as the surface area of the heated surface is

several orders of magnitude smaller than the available surface area to radiate heat to. A "viewing angle" must be taken into account when the heat cannot be radiated in every direction due to a surface at the same temperature as the heated surface. Not only does this greatly increase the difficulty of the heat transfer calculations, but it also always has a negative effect on the radiant heat transfer rate. Therefore, it is desirable to avoid designs falling outside the criterion for simple radiant heat transfer.

This system is very attractive for its sheer simplicity. With no moving parts there are far fewer chances for something to malfunction or fail during operation. A basic operational system, as shown below in Figure 8, would simply be composed of the tungsten plane, a vacuum container for the slab, and a magnetic sweep to remove the electrons from the beam path before striking the molybdenum slug. The vacuum container would probably be cooled by a flow of water to maintain low temperature, but over such a large surface area a tap fed flow would be sufficient.

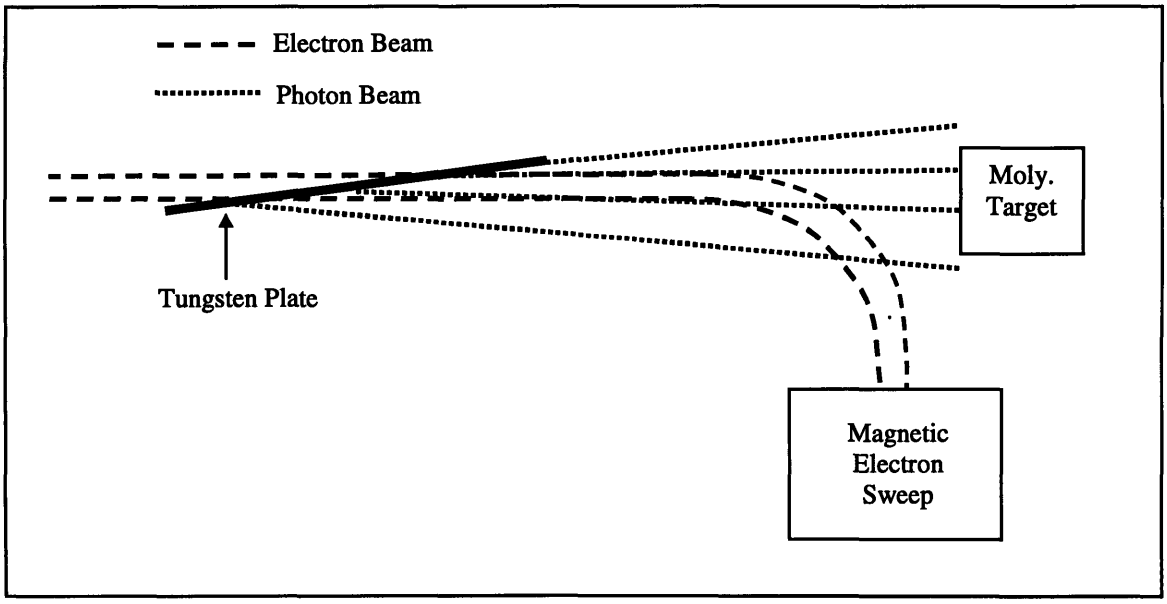

FIGURE 8: BASIC SYSTEM DESIGN FOR RADIANTLY COOLED CONVERTER

4.1.1 FOUR BASIC MODELS

Four basic models were considered in the initial part of this study. Inclined planes 1 cm wide and with horizontal lengths of 5 cm, 10 cm, 15 cm, and 20 cm where chosen for analysis. The planes are of the appropriate thickness to give an equivalent horizontal thickness of 0.30 cm. The maximum allowable heat deposition rate for each plane is then determined using the formula outlined in section 2.3.2 to maintain its surface temperature at 3000K. A summary of these design parameters is given below in Table I. The name for each model is determined by three design factors: horizontal length, equivalent thickness, and electron beam energy. For instance, S103045 is a model that has a horizontal length of 10 cm, an equivalent thickness of 0.30 cm, and a electron beam energy of 45 MeV. These are the primary variables that will be used to optimize the radiantly cooled converter.

TABLE I: PHYSICAL PARAMETERS FOR 4 BASIC RADIANT TRANSFER MODELS

Name	Length(cm)	Thickness(cm)	Equivilent Thickness(cm)	Area(cm^2)	Max. Heat Deposition (w)
S053045	5	0.0588	0.30	10	1100
S103045	10	0.0299	0.30	20	2150
S153045	15	0.0200	0.30	30	3250
S203045	20	0.0150	0.30	40	4300

Each of these was analyzed using MCNP to model the electron and photon interactions occurring within the model. The input deck for S053045 is given in Appendix B as an example. There are several issues regarding how MCNP was used to model these cases that should be considered when analyzing the results. First, to insure errors of less than 5% for the desired tallies, 25000 particle histories were performed for each model. This number of histories kept the statistical error fairly low while allowing the models to run in a time of 10 to 20 minutes each on a Pentium-200MMX computer.

Increasing the number of case histories performed could reduce the errors but this can have a drastic effect on the run-time for the model. To decrease the error by a factor of 2, the number of source particles must be increased by a factor of 4. Second, to reduce the run-time for the models, energy cut-offs for low energy particles where utilized at a number of points in the analysis. A cut-off point of 0.5 MeV was chosen for both electrons and photons. This value was chosen as a balance between two extremes. On the one side, there is cutting off all particles below 8 MeV since they can no longer contribute to the GDR region. On the other side, is not cutting off low energy particles at all to more accurately model the heat deposition rates in the materials. The value of 0.5 MeV was chosen because no substantial change in the heat deposition rate was noted with lower cut-off points. Finally, the electron importance in the region between the converter and the molybdenum slug is set to zero. This was done to model the effects of a magnetic electron beam sweep. This magnetic sweep will effectively bend the entire electron beam away from the molybdenum slug while leaving the produced photon beam unaffected. Therefore no electrons will strike the molybdenum target, dramatically reducing the heat deposition rate in the target.

The first step in any modeling procedure is to insure that the model is giving an accurate picture of what is really going on. One simple check of an MCNP model is to perform an energy balance. The total amount of energy that goes into a system must be accounted for, either in energy leaving the system or by energy deposited into some portion of the model itself. The only energy entering the system is from the incident electron beam. For the basic cases analyzed here, this amounts to 45 MeV of Energy. There are four possible ways for this energy to be accounted for: electrons leaving the

system, photons leaving the system, electron and photon energy absorbed in the tungsten converter, and photon energy absorbed by the molybdenum target. The sum of these four should equal the 45 MeV. The energy balances for the four basic models are shown below in Table II.

TABLE II: ENERGY BALANCES FOR THE BASIC MODELS

Name	Escape Electrons	Escape Photons	Converter Absorbed	Target Absorbed	Total (MeV)
S053045	23.43	14.33	6.87	0.23	44.86
S103045	29.64	10.89	4.18	0.17	44.88
S153045	32.84	8.92	3.01	0.14	44.90
S203045	34.87	7.56	2.37	0.12	44.92

The total values show that all the energy going into the model is being accounted for, either through escape or absorption, within an acceptable statistical variance. From this it can be inferred that the model is running correctly and no unforeseen reactions are occurring within the model. These results also show that the shorter converters are substantially better at producing photons.

There are several key factors that need to be considered when analyzing the results of the radiantly cooled converter models. The Yield of the model shows the models efficiency at converting electrons to on target GDR photons at a given beam current. The heat deposition is the number of MeV absorbed by the converter out of the incident beam energy, in this case 45 MeV. The heat deposition is one of two factors that can limit the allowable beam current for the model. The maximum allowable heating for each converter length is determined using the method outlined in section 2.3.2. The maximum allowable heating is then divided by the heat deposition, giving the maximum allowable current for the electron beam (max $beam_1$, below). The second factor limiting beam current is the accelerator itself. The maximum beam current at a given electron

energy is taken from Figure 2. The smaller of these two values (max $beam_1$ and max $beam_2$, below) is therefore the maximum allowable beam current. The yield for each model is then multiplied by the ratio of the maximum allowable beam current over the beam current for the slug model (250μA) to give the current weighted yield. These results are summarized in Table III below.

TABLE III: SUMMARY OF RESULTS FOR 4 BASIC MODELS

Conv. Length	Yield (mb/cm^2)	Error	Heat Dep. (MeV)	Error	Max. Heat (W)	Max. $Beam_1$ (μA)	Max. $Beam_2$ (μA)	Beam Current (μA)	Current Yield
5	2.349	0.099	6.867	0.027	1100	160	575	160	1.505
10	1.610	0.082	4.179	0.020	2150	514	575	514	3.314
20	1.166	0.069	3.009	0.017	3250	1080	575	575	2.681
30	0.946	0.062	2.371	0.014	4300	1813	575	575	2.177

The 10-centimeter long converter plate shows the best performance out of the four. This is due to the fact that it strikes a balance between yield and beam current. The 5-centimeter model has a higher yield, but it also has a higher heat deposition. This combined with a lower allowable heating mean that the 5-centimeter model must be operated at a lower current. The longer converters, 20 and 30-centimeters suffer from the opposite problem. They are able to dissipate more heat then the accelerator is capable of generating, therefore yield cannot be increased by increasing the current. By adjusting the energy of the electron beam and the thickness of the converter it is possible to manipulate these results. However, these changes have a much larger effect on the heating of the converter than on the yield in the molybdenum target. Therefore, only the 5 and 10-centimeter length converters were chosen for further study.

4.1.2 VARIATION OF PLATE THICKNESS

The first parameter chosen for optimization was the converter plate equivalent thickness. This is not the true thickness of the converter plate, but the horizontal distance

through the plate when it is positioned at the designated angle. This "thickness" is therefore the length of tungsten the electron beam must pass through when it strikes the converter plate. The results will show that, to a point, as the equivalent thickness of the slab decreases the yield in the molybdenum slug increases.

However, care must be taken in reducing the thickness of the converter. The converter is going to operating at temperatures approaching 3000K. Even though tungsten's melting point is over 3600K, this temperature is high enough such that the issues of heat warping become a significant concern. If the converter is too thin its strength will be decreased and as its temperature rises it can begin to warp. When changes in equivalent thickness of 0.01-centimeter can have a substantial effect on system performance, the warping of the converter plate must obviously be kept to a minimum. For this reason a minimum plate thickness of 0.01-centimeter was chosen for the converter plates designs. Verification of plate integrity at full power should be one of the first items addressed in an experimental setup based on this design.

The effect of varying the equivalent thickness of the converter plate was studied over a range of possible values. The minimum equivalent thickness' for the 5 and 10-centimenter designs, 0.05-centimeter and 0.10-centimeter respectively, were determined by the 0.01-centimter minimum thickness requirements outlined above. The maximum thickness for each was chosen by taking 40% the range of 45 MeV electrons in tungsten:

$$0.40 \cdot \text{Range(cm)} = 0.40 \cdot \frac{\text{Energy (MeV)}}{2 \cdot \text{Density}\left(\frac{\text{g}}{\text{cm}^2}\right)} = 0.40 \cdot \frac{45}{2 \cdot 19.3} = 0.467\text{(cm)} \approx 0.50\text{(cm)}$$

The range between the maximum and minimum plate thickness was then divided by the appropriate number of segments so that there was a 0.05-centimeter difference in each

model. All of the calculations were performed with the electron beam energy set to 45 MeV. The results for these models are shown below in Table IV for the 5-centimeter model and in Table V for the 10-centimeter model.

TABLE IV: RESULTS FOR VARYING THICKNESS ON 5-CM CONVERTER PLATE

Conv. Thickness	Yield (mb/cm^2)	Error	Heat Dep. (MeV)	Error	Max. Heat (W)	Max. $Beam_1$ (μA)	Max. $Beam_2$ (μA)	Beam Current (μA)	Current Yield
0.05	1.941	0.089	1.349	0.009	1100	575	816	575	4.463
0.10	2.468	0.102	2.679	0.014	1100	575	411	411	4.054
0.15	2.480	0.102	3.842	0.018	1100	575	286	286	2.840
0.20	2.385	0.098	4.944	0.021	1100	575	222	222	2.122
0.25	2.321	0.098	5.951	0.024	1100	575	185	185	1.716
0.30	2.349	0.099	6.867	0.027	1100	575	160	160	1.505
0.35	2.270	0.097	7.783	0.030	1100	575	141	141	1.283
0.40	2.147	0.094	8.606	0.033	1100	575	128	128	1.097
0.45	2.013	0.090	9.433	0.035	1100	575	117	117	0.939
0.50	1.892	0.088	10.209	0.038	1100	575	108	108	0.815

TABLE V: RESULTS FOR VARYING THICKNESS ON 10-CM CONVERTER PLATE

Conv. Thickness	Yield (mb/cm^2)	Error	Heat Dep. (MeV)	Error	Max. Heat (W)	Max. $Beam_1$ (μA)	Max. $Beam_2$ (μA)	Beam Current (μA)	Current Yield
0.10	1.757	0.086	1.972	0.012	2150	575	1090	575	4.040
0.15	1.850	0.088	2.606	0.014	2150	575	825	575	4.256
0.20	1.829	0.087	3.176	0.016	2150	575	677	575	4.207
0.25	1.744	0.085	3.696	0.018	2150	575	582	575	4.010
0.30	1.610	0.082	4.179	0.020	2150	575	514	514	3.314
0.35	1.636	0.083	4.633	0.022	2150	575	464	464	3.037
0.40	1.548	0.080	5.078	0.023	2150	575	423	423	2.621
0.45	1.543	0.081	5.487	0.025	2150	575	392	392	2.418
0.50	1.405	0.077	5.907	0.027	2150	575	364	364	2.046

These results show that varying the equivalent thickness of the converter plate can have a substantial effect on the on the amount of energy absorbed. The decreasing absorbed energy allows the beam current to be increased, which raises the current weighted yield in the molybdenum slug. The models showed the 0.05-cm thick 5-cm converter plate to have the best results with a current weighted yield of 4.463-mb/cm^2; the 0.15-cm thick 10-cm converter plate was close behind with a current weighted yield of 4.256-mb/cm^2.

4.1.3 VARIATION OF ELECTRON BEAM ENERGY

The second parameter chosen for optimization was the energy of the accelerated electron beam. As outlined in section 1.2, the LINAC produced electron beam used in this study is capable of operation over a variety of electron energies and beam currents. The relationship between electron energy and maximum beam current is a linear one, with current decreasing as electron energy increases. The results will show that as the electron beam energy goes up, so does the yield in the molybdenum slug.

However, since the heat transfer properties of the system are so closely related to the nuclear properties there is a far more complex relationship between electron beam energy and optimum current weighted yield in the molybdenum target. As the electron beam energy goes up the yield in the molybdenum target goes up, but the amount of heat deposited in the converter goes up as well. For each length of the converter, there is a limited amount of heat the converter is able to radiate. Therefore, at lower electron energies, where the allowable current can be very large, the beam current is typically limited by the heat deposition in the converter. At higher electron energies, where the allowable current is relatively small, the beam current is typically limited by the specifications of the LINAC. Sensitivity studies have shown that a balance is struck between the heat transfer capabilities of the converter and the increased yield of the high energy electrons when the maximum allowable beam current determined by the heat transfer parameters is approximately 1.2 times the maximum allowable beam current determined by the LINAC parameters. This relationship is only noticeable in converter plates with relatively thin equivalent thickness. The relation exists for the thicker plates as well, but the energy at which the maximum occurs is higher than the LINAC used here is capable of producing. The relationship also shows that as the converter plate thickness

increases the maximum possible current weighted yield in the molybdenum target decreases.

The effect of electron beam energy was studied over the entire range of operation for the LINAC, at 5 MeV intervals from 30 MeV to 60 MeV. All models were designed with a converter plate equivalent thickness of 0.30-cm. The results for these models are shown below in Table VI for the 5-cm converter plate model and in Table VII for the 10-cm converter plate model.

TABLE VI: RESULTS FOR VARYING ENERGY ON 5-CM CONVERTER PLATE

Electron Energy (MeV)	Yield (mb/cm2)	Error	Heat Dep. (MeV)	Error	Max. Heat (W)	Max. $Beam_1$ (μA)	Max. $Beam_2$ (μA)	Beam Current (μA)	Current Yield
30.00	1.078	0.066	5.293	0.021	1100	950	208	208	0.896
35.00	1.369	0.075	5.857	0.023	1100	825	188	188	1.028
40.00	1.965	0.089	6.400	0.026	1100	700	172	172	1.351
45.00	2.349	0.099	6.867	0.027	1100	575	160	160	1.505
50.00	2.648	0.105	7.315	0.029	1100	450	150	150	1.593
55.00	3.381	0.121	7.687	0.031	1100	325	143	143	1.935
60.00	3.700	0.125	7.987	0.033	1100	200	138	138	2.038

TABLE VII: RESULTS FOR VARYING ENERGY ON 10-CM CONVERTER PLATE

Electron Energy (MeV)	Yield (mb/cm2)	Error	Heat Dep. (MeV)	Error	Max. Heat (W)	Max. $Beam_1$ (μA)	Max. $Beam_2$ (μA)	Beam Current (μA)	Current Yield
30.00	0.800	0.058	3.065	0.015	2150	950	702	702	2.245
35.00	0.965	0.063	3.467	0.017	2150	825	620	620	2.394
40.00	1.345	0.073	3.869	0.019	2150	700	556	556	2.991
45.00	1.610	0.082	4.179	0.020	2150	575	514	514	3.314
50.00	1.941	0.090	4.515	0.021	2150	450	476	450	3.495
55.00	2.384	0.102	4.831	0.023	2150	325	445	325	3.099
60.00	2.634	0.107	5.125	0.024	2150	200	420	200	2.107

These results show that the variation of electron beam energy has a more subdued effect on current weighted yield than does the variation of converter plate equivalent thickness. This is not to say that the effect is unimportant, at a given thickness the variation of electron energy can change the current weighted yield by as much as 227%,

as is the case of the 5-cm converter plate. This effect decreases with increased converter length, the 10-cm converter plate shows a variance of only 166%.

The variation of electron beam energy was next applied to the optimum converter plate equivalent thickness models from section 4.1.2 to ensure that the final design was at not only its optimum thickness but its optimum electron beam energy as well. Both the 5-cm and 10-cm converter plate models were analyzed with electron beam energies of 30-50 MeV. The results for these models are shown below in Table VIII for the 5-cm converter plate model and in Table IX for the 10-cm converter plate model.

TABLE VIII: RESULTS FOR VARYING ENERGY ON OPTIMIZED 5-CM PLATE

Electron Energy (MeV)	Yield (mb/cm2)	Error	Heat Dep. (MeV)	Error	Max. Heat (W)	Max. $Beam_1$ (μA)	Max. $Beam_2$ (μA)	Beam Current (μA)	Current Yield
30.00	1.050	0.063	1.291	0.006	1100	950	852	852	3.578
35.00	1.407	0.055	1.333	0.007	1100	825	825	825	4.643
40.00	1.755	0.049	1.335	0.007	1100	700	824	700	4.913
45.00	1.941	0.046	1.349	0.007	1100	575	816	575	4.463
50.00	2.189	0.044	1.352	0.007	1100	450	814	450	3.939

TABLE IX: RESULTS FOR VARYING ENERGY ON OPTIMIZED 10-CM PLATE

Electron Energy (MeV)	Yield (mb/cm2)	Error	Heat Dep. (MeV)	Error	Max. Heat (W)	Max. $Beam_1$ (μA)	Max. $Beam_2$ (μA)	Beam Current (μA)	Current Yield
30.00	0.897	0.061	2.003	0.011	2150	950	1074	950	3.408
35.00	1.033	0.064	2.229	0.012	2150	825	965	825	3.408
40.00	1.523	0.078	2.455	0.013	2150	700	876	700	4.264
45.00	1.850	0.088	2.606	0.014	2150	575	825	575	4.256
50.00	2.071	0.094	2.804	0.015	2150	450	767	450	3.728

These results show that the 5-cm converter plate outperforms the 10-cm converter plate by approximately 15% at optimized electron beam energy and converter plate equivalent thickness. These models also support the observation that maximum current weighted yield occurring when the ratio of max $beam_1$ to max $beam_2$ is 1.2 in value. The optimum single plate design will therefore be based upon the 5-cm converter plate model, with equivalent thickness of 0.05 cm and electron beam energy of 40 MeV.

4.1.4 Optimum Single Inclined Plane Converter Design

The optimum single inclined plane converter design was determined to be a 5-cm converter plate model with an equivalent thickness of 0.05-cm and electron beam energy of 40 MeV. This results in a yield of 1.755±0.049 mb/cm^2 in the molybdenum slug. A graph of the yield contribution over the GDR energy range is shown below in Figure 9.

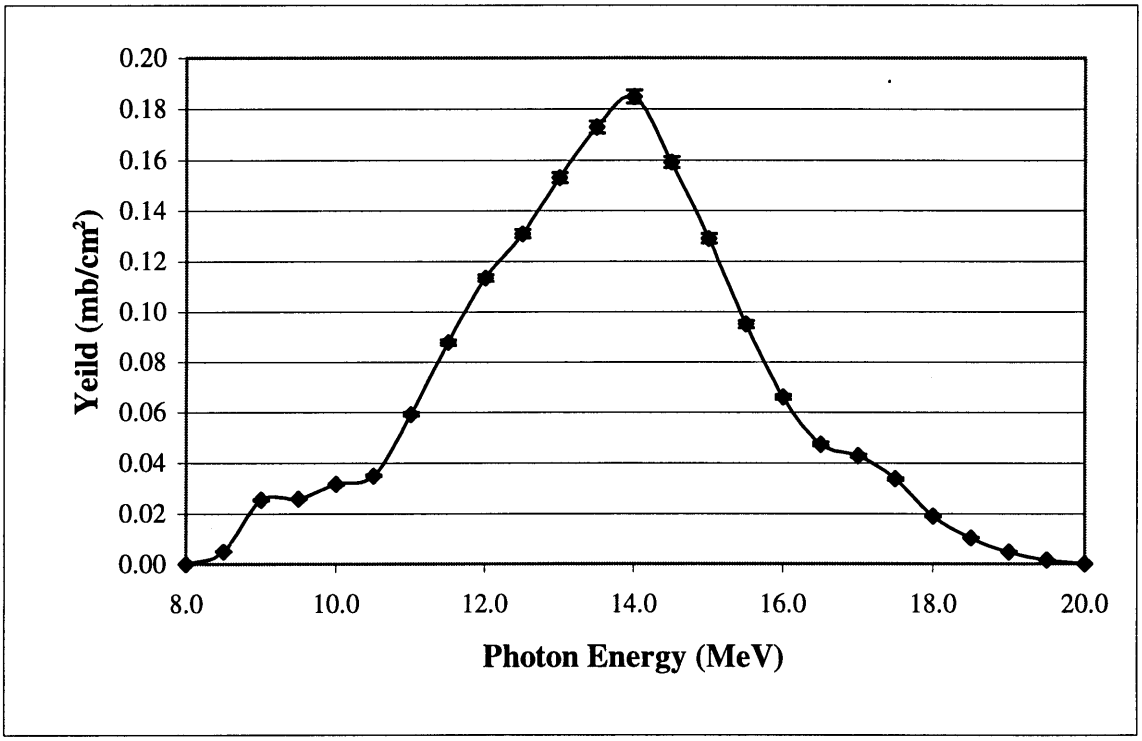

Figure 9: Yield for the Optimum Inclined Plane Model

For this case the maximum beam current is determined by the specifications of the LINAC electron accelerator, see Table VIII. To produce 40 MeV electrons the accelerator can be set to a maximum current of 700 μA. Therefore a current weighted yield of 4.914±0.137 mb/cm^2 is produced in the molybdenum slug. This also results in the deposition of approximately 935 watts of power into the tungsten converter. According to the simple radiant heat transfer model this would result in a surface temperature of 2903K. The full temperature profile for the slab, calculated in the

spreadsheet model, determined the peak temperature to be 2873K. This reduced temperature is due to the conduction of heat to areas of the rectangular slab not directly exposed to the electron beam. A graph of the temperature profile for one quadrant of the slab is shown below in Figure 10.

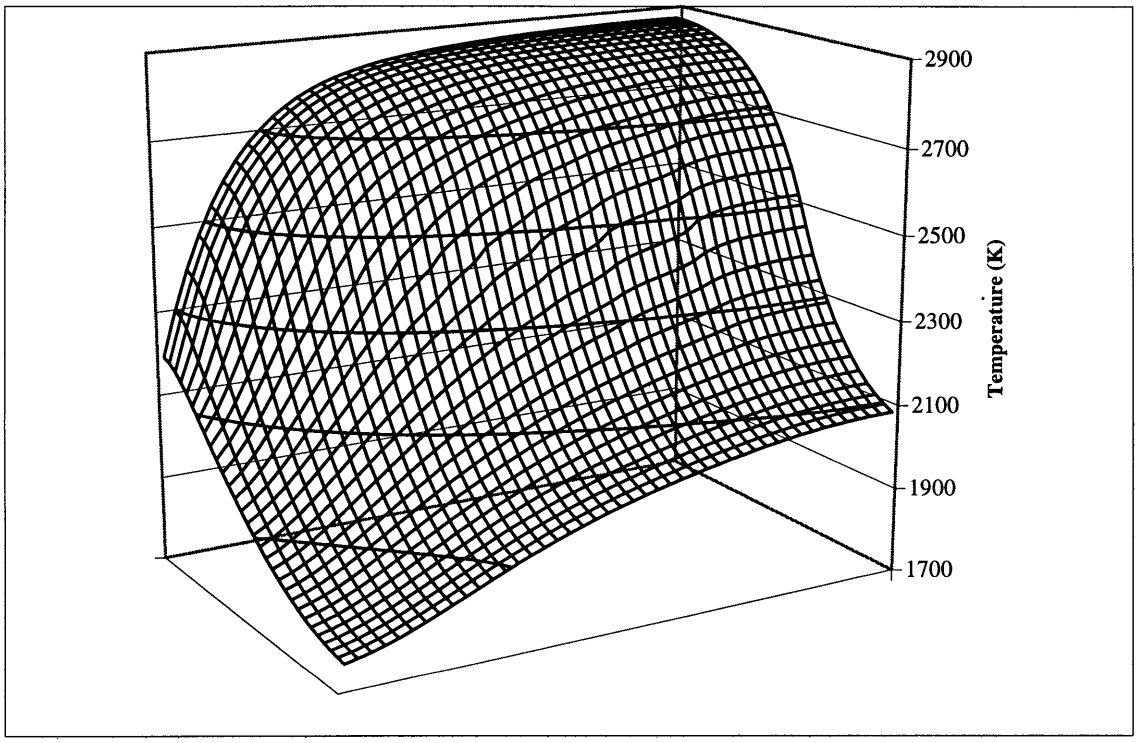

FIGURE 10: TEMPERATURE PROFILE FOR OPTIMUM SINGLE PLATE CONVERTER

4.2 MULTIPLE INCLINED PLANES OF TUNGSTEN

The multiple plane model was originally conceived for the purpose of increasing the surface area of the converter for radiant heat transfer. By increasing the heat transfer of the system the beam current could be raised and the current weighted yield would increase. In retrospect, with the limiting factor of the beam current for the single plane model being the specification for the LINAC, the reasoning is flawed. The results for the

multiple plane model clearly show that the single inclined plane design has far superior performance characteristics.

The following multiple plane model is based on the optimum single plane design discussed in the previous section and is in fact the optimum two plane design. It is a two-plane model with a total length of 5-cm and an equivalent thickness of 0.05-cm. Table X below shows the basic results for the model.

TABLE X: RESULTS FOR TWO-PLANE MODEL

Electron Energy (MeV)	Yield (mb/cm2)	Error	Heat Dep. (MeV)	Error	Max. Heat (W)	Max. $Beam_1$ (μA)	Max. $Beam_2$ (μA)	Beam Current (μA)	Current Yield
40.00	1.330	0.052	1.724	0.008	1160	700	673	673	3.579

As can be seen from the table the maximum beam current for the model is determined by the heat deposition and not by the LINAC parameters. A thinner plate would have decreased the amount of absorbed heat and increased the current yield, but this also would have violated the design parameter of 0.01-cm minimum thickness for the tungsten plate. It should also be noted that the heat transfer modeling of this system did not include the effects of viewing angle on the radiant heat transfer. The angle created by the two plates would have necessitated the use of a viewing angle when calculating radiant heat transfer, thereby decreasing the allowed heat deposition and current weighted yield in the molybdenum slug. Due to its initial poor results this model was quickly abandoned for more promising converter designs.

4.3 SINGLE CONE OF TUNGSTEN

When the incident electron beam creates the bremsstrahlung photons their scattering angle from the direction of the beam is directly related to their energy. The higher the energy the smaller the scattering angle. This is to the advantage of this

production system since high-energy photons are desired and low-energy ones are not. This basic idea was the foundation to the radiantly cooled cone model. The cone is pointed in the direction of the electron beam. Therefore, the tip of the cone is closest to the molybdenum target. The high-energy, small angle photons produced in the tip of the cone therefore have a much higher probability of striking the molybdenum target.

The initial converter model was a 10-cm long cone with an equivalent thickness of 0.10-cm. The electron beam energy was set to 40 MeV. The model had a yield of 1.450±0.089 mb/cm^2 and an energy deposition of 1.632±0.011 MeV. At first glance these numbers appear very similar to the single plane results. However, there are some very substantial differences. The surface area for a cone is determined by the following equation:

$$\text{Area} = \pi \cdot r^2 + \pi \cdot r \cdot \sqrt{r^2 + h^2}$$

Therefore the surface area of the cone is only 11.6-cm^2. To ensure that temperature peaking in the tip of the cone doesn't melt the tungsten an average surface temperature of 2750K was chosen. At this surface temperature the cone would only be able to dissipate approximately 900 watts of power. This would allow a maximum beam current of only 550 μA. The current weighted yield produced is therefore 3.199±0.196 mb/cm^2, which is significantly lower than the single plane converter. A second design that was 20-cm long cone was also modeled. The increased surface area allowed a maximum heat deposition of approximately 1500 watts. Since the heat deposition was only 1.11 MeV, the beam current was limited by the LINAC parameters to 700 μA. Unfortunately, the yield for the longer cone was only 0.654±0.061 mb/cm^2. Therefore, despite the higher beam current, the current weighted yield for the model was only 1.831±0.171 mb/cm^2.

At this point the cone model was abandoned for two primary reasons. The first is construction difficulty. As difficult as it may be to fabricate the single plane converter, a cone as thin as the ones described here would be even more difficult. As the cone's temperature rose it may very well collapse on itself from lack of strength. The second reason is a difficulty in the heat transfer model. The radiant heat transfer in the slab models was improved by simply extending the plane wider than the electron beam spot, thereby increasing the available surface area for heat transfer. This simply isn't possible with the cone model.

4.4 System Optimum Design and Limitations

It was therefore concluded, that for radiantly cooled converters the single inclined plane was the most efficient and effective design of those analyzed. The optimum single plane design studied was a 5-cm long plate with an equivalent thickness of 0.05-cm. This design produced a current weighted yield of 4.914±0.137 mb/cm^2, close to an 80% increase over the PHMX case yield of 2.738±0.033 mb/cm^2. However, these systems are still severely limited by the low heat transfer rate of radiant cooling. They simply wouldn't be effective for ultra-high yield systems.

5. MOLTEN LEAD CONVERTER ANALYSIS

5.1 BASIC DESIGN

The basic reason for using a molten lead converter is the increased heat transfer capabilities of the molten lead system. The radiant converter is very limited in the amount of heat it can reject. To increase its heat transfer you must increase the size of the converter, which tends to decrease the produced flux on target. This is a result of the interdependence of the heat transfer and nuclear properties in the radiantly cooled converter system. However, the molten lead converter is very different. The heat transfer aspect and the nuclear aspect of the system are almost wholly independent. Therefore, the system can be optimized to produce the largest possible flux on target without considering the amount of heat that the lead is absorbing. Once the nuclear aspect of the system has been optimized the heat transfer aspect can simply be scaled to the amount of absorbed heat in the lead.

The design for the circulating molten lead loop is relatively straightforward. The molten lead is circulated through a duct of corrosion resistant stainless steel by a high flow rate pumping system. At one point in the loop, the converter, the absorbed heat from the electron beam heats the lead. The lead is then circulated through a heat exchanger where the heat is transferred to another cooling medium, most likely water. Since the melting temperature of lead is well above the boiling temperature of water at atmospheric pressure, the two fluids will be separated by a thick plate of metal to act as a buffer between them. This buffer will have appropriate thickness and conductivity to create a temperature gradient between the two fluids such that there will be no concern over spot freezing in the lead or spot boiling in the water. After going through the pump,

the lead starts the entire cycle again. A basic diagram of such a system is shown below in Figure 11.

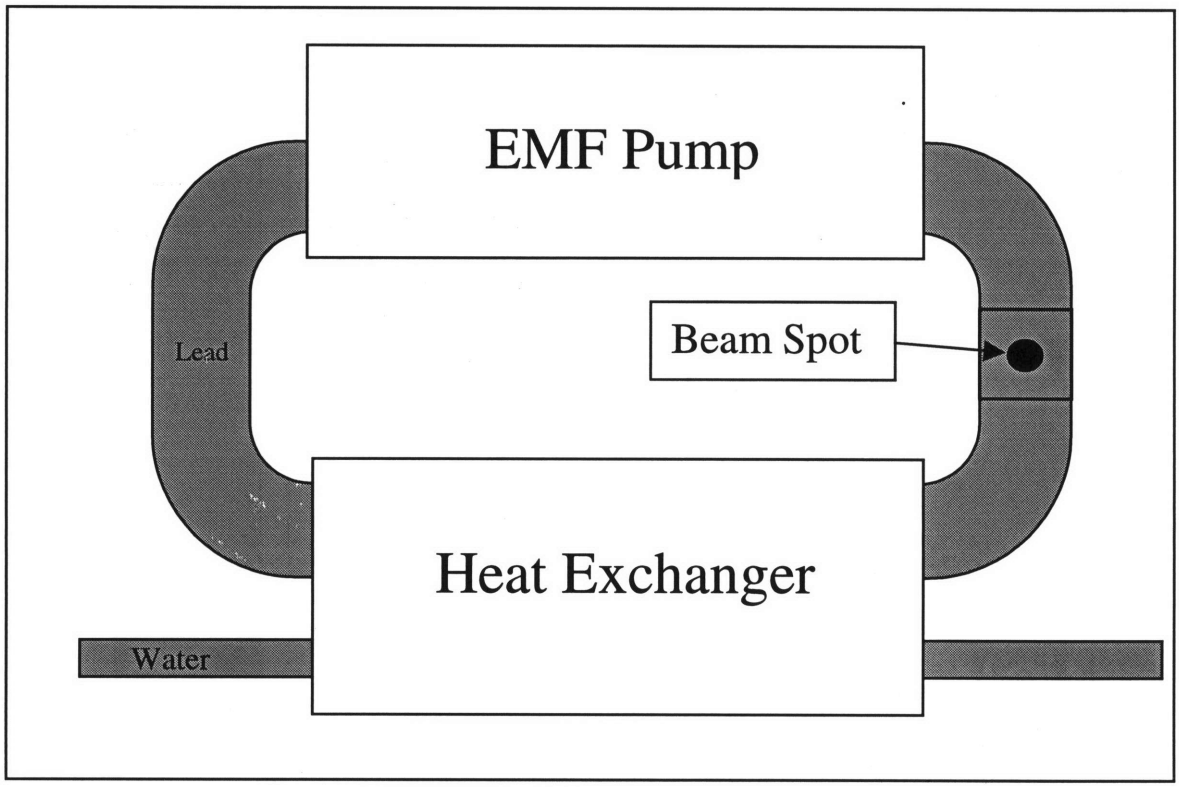

FIGURE 11: BASIC DIAGRAM OF MOLTEN LEAD CONVERTER SYSTEM

The MCNP model used to study the molten lead system is based only on the actual converter section of the molten lead loop. The rest of the molten lead loop doesn't play a role in the nuclear analysis and will therefore not be modeled. The 4-cm by 1-cm cross-sectional duct used for the molten lead flow will be narrowed to the specified thickness of the target in the in the converter section. The stainless steel duct will also be thinned to approximately .05 cm in thickness in the exact area of the converter that the beam will be striking. This will reduce the interaction between the stainless steel and both the incident electron beam and the produced photon beam. To maintain consistency with the other models the molybdenum target will be modeled as a 1-cm diameter by 1-cm long slug of pure ^{100}Mo placed 5-cm from the outer edge of the stainless steel duct.

The importance for electrons in the molybdenum slug will be zero in order to simulate the effects of a magnetic electron sweep. The MCNP input deck for this model is given in Appendix A. A basic diagram of the converter section is shown below in Figure 12.

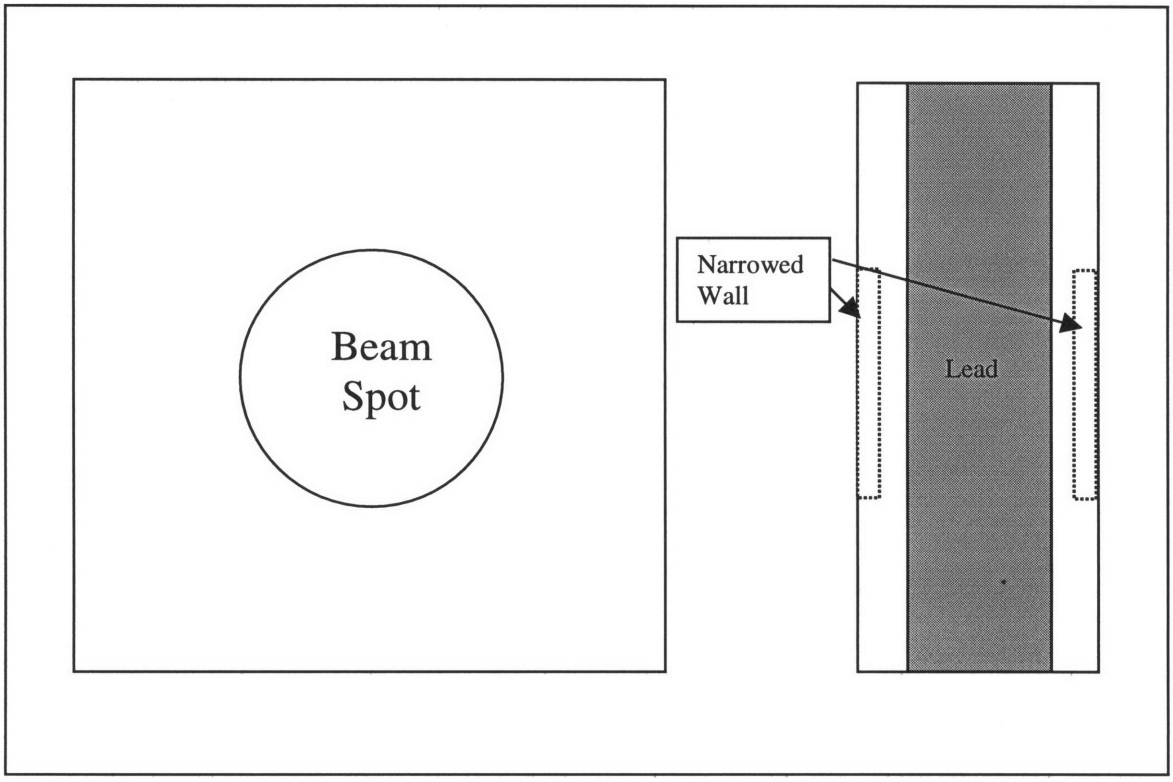

FIGURE 12: THE CONVERTER SECTION OF THE MOLTEN LEAD LOOP

The rest of chapter 5 is devoted to the modeling and optimization of the nuclear aspects for the molten lead converter system. The pumping, heat exchange, and other converter loop systems will be discussed in detail in chapter 6.

5.2 MCNP Analysis and Design Performance

There are two parameters that can be varied in order to optimize the GDR photon flux on target for the molten lead converter: the electron beam energy and the thickness of the lead flow. The optimum electron energy is determined primarily by two factors. The first is spectrum of photons created by the electron beam. The energy spectrum of the photon beam produced by the lead converter is determined by the energy of the incident electron beam. The second factor determining the optimum electron energy is the allowable current for the accelerator at such energy. The accelerator is capable of operating at significantly higher currents at low beam energy than at high beam energy. The current acts as a direct linear multiplier to the yield in the molybdenum slug; therefore the positive effects on yield by increasing the electron energy must be balanced with the decreasing current. The optimum lead thickness is slightly more difficult to define. There are two competing effects occurring within the lead converter, as there are in any target. The first effect is that as the target increases in thickness the number of incident electrons converted to photons increases. However, as the thickness increases the number of photons that are either scattered out of the target path or absorbed also increases. To determine the optimum thickness these two effects need to be balanced.

The initial model's lead thickness and electron energy were determined by analyzing the results of the PHMX slug case. Bremsstrahlung production goes as Z^2, therefore an initial estimate for the optimum thickness is given by:

$$\text{PB (cm)} = \text{W (cm)} \cdot \frac{Z_W^2}{Z_{Pb}^2} = 0.35\text{cm} \cdot \frac{74^2}{82^2} = 0.285\text{cm}$$

Since the model was going to be analyzed over a variety of configurations, the starting thickness was rounded to a value of 0.30-centimeters. The energy of the electron beam

was chosen to be 40 MeV, the same as the PMHX slug case. This was chosen because of the photon spectrum it produces and the current at which the accelerator can be run at that energy. At 40 MeV the accelerator can be run at 700 μA, which generates a beam power of approximately 28 kilowatts. Since heat deposition isn't a concern this should help to maximize photon production.

Once again, the first step with any new MCNP model is to perform an energy balance to ensure that it is running properly and giving an accurate description of the system in question. There are five different possible end points for energy entering this system: electrons leaving the system, photons leaving the system, and heat deposition in the lead, molybdenum, or stainless steel. The results for the energy balance are given below in Table XI.

TABLE XI: ENERGY BALANCE FOR INITIAL LEAD CONVERTER MODEL

Escape Electrons	Escape Photons	Absorbed Lead	Absorbed Moly.	Absorbed S.S.	Energy (MeV)
18.52	12.64	6.04	1.38	1.39	39.97

As can be seen in the table, all of the energy entering the system model is accounted for either by escape particles or absorbed energy. Therefore, it can be assumed that the model is running properly and that the results are accurate.

The initial model produced a yield of 2.993±0.025 mb/cm^2 in the molybdenum slug. This increase is due primarily to improved bremsstrahlung production in lead versus tungsten. Assuming that the accelerator is run at maximum current for the lead target, the current weighted yield would be 8.381±0.070 mb/cm^2, a substantial improvement over both the baseline PMHX slug converter and the optimized radiantly cooled slab

converter. The next step is to optimize the lead thickness and beam energy for the converter.

First the optimum electron beam energy was determined. This was performed by running the same model as above at the additional beam energies of 30, 35, 45, and 50 MeV. The higher electron beam energies, 55 and 60 MeV, were not modeled because previous experience with the tungsten based converter show that the lower allowable beam currents associated with high electron energies always negate the increased yield. The results for these models are given below in Table XII.

TABLE XII: RESULTS FOR VARYING ENERGY ON MOLTEN LEAD CONVERTER

Electron Energy (MeV)	Yield (mb/cm^2)	Error	Current (μA)	Current Yield	Error
30	1.772	0.019	950	6.733	0.072
35	2.327	0.022	825	7.679	0.071
40	3.024	0.025	700	8.468	0.070
45	3.612	0.027	575	8.307	0.063
50	4.230	0.030	450	7.615	0.053

As Table XII shows the reasoning outlined above for determining the optimum electron beam energy appears to be fairly accurate. The yield for beam energy of 45 MeV is very close to the yield for 40 MeV and therefore the true optimum probably lies somewhere between the two values.

The next step was to optimize the lead thickness for the energy of the electron beam. During analysis of the tungsten target several patterns in performance were noted that lead to a more efficient design than was readily apparent. Therefore, even though the optimum energy for electron conversion has been approximated, the thickness of the lead converter will be varied for the entire range of possible electron energies. Therefore, if there are any secondary relationships occurring within the model, they should be

discernable from the data. The results for the yield in the molybdenum are given below in Table XIII.

TABLE XIII: YIELD FOR RANGE OF LEAD CONVERTER MODELS

Energy (MeV)	Thickness(cm)				
	15	20	25	30	35
30	1.802	1.817	1.797	1.772	1.730
35	2.330	2.392	2.375	2.327	2.269
40	2.956	3.008	3.032	3.024	2.963
45	3.486	3.581	3.620	3.612	3.548
50	4.009	4.181	4.253	4.230	4.175

These results agree with the ones presented in Table XII above, in that as electron beam energy goes up so does the yield in the molybdenum target. The results also show that for the lead converter the yield is relatively insensitive to the thickness of the lead. Maximums do exist, mostly in 0.20 to 0.25-cm range, but the variance of the yield over the range of lead thickness is relatively minor. By multiplying the yields by the appropriate current for the electron beam energy a more accurate picture of the optimum configuration is produced. These results are shown below in Table XIV.

TABLE XIV: CURRENT WEIGHTED YIELD FOR RANGE OF LEAD MODELS

Energy (MeV)	Thickness(cm)				
	15	20	25	30	35
30	6.849	6.906	6.827	6.733	6.573
35	7.689	7.892	7.836	7.679	7.488
40	8.278	8.422	8.490	8.468	8.298
45	8.018	8.237	8.327	8.307	8.161
50	7.217	7.525	7.655	7.615	7.514

Table XIV gives a clearer picture of the relationship between electron energy, beam current, and yield optimization. The estimates used to pick the initial lead model, which were based on the optimum tungsten slug model, predicted a model with a electron beam energy of 40 MeV and a lead converter thickness of 0.285 cm. These initial estimates

were in fact quite accurate. The MCNP model determined the optimum configuration for the target to be an electron energy of 40 MeV and a lead converter thickness of 0.25-cm.

5.3 Optimum Molten Lead Converter Design

The molten lead converter with the highest current weighted yield was determined by a series of sensitivity studies. These studies found that an electron beam energy of 40 MeV and a molten lead thickness of 0.25-cm produces the largest current weighted yield in the molybdenum target. The current-weighted yield for the design was determined to be 8.457±0.023 mb/cm^2, substantially higher than either the PMHX slug case or the radiantly cooled plate designs. The yield contributions over the GDR energy range are shown below in Figure 13.

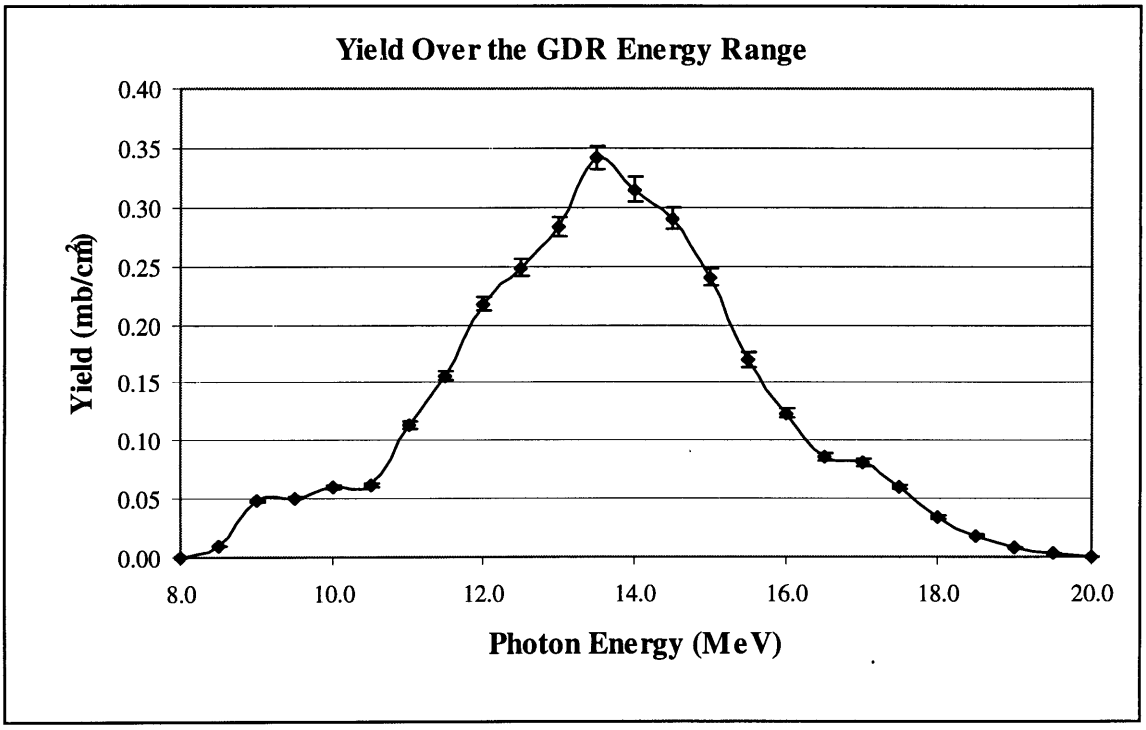

Figure 13: The Yield for the Optimum Molten Lead Converter

This increased yield was due primarily to the lead systems ability to handle an increased heat load. The PMHX slug and radiantly cooled plate are limited by the heat rejection parameters of their design, while the lead system can simply be scaled to reject the extra energy deposited. Therefore, the lead converter can be used with the beam current set at its maximum value. However, even without this added effect the lead converter is slightly more efficient at producing a useable photon flux on target. This is a result of lead's higher Z number, since an element's Z number is one of the primary factors in determining bremsstrahlung photon production.

As previously stated the cooling system for the molten lead target is essentially independent of the actual electron-to-photon converter design. This is not to say that it is unimportant though. The pumping and heat exchange systems are central to the successful operation of a circulating molten lead target. These systems are explored in detail in the following chapter.

6. MOLTEN LEAD CONVERTER SYSTEM DESIGN

6.1 BASIC CIRCULATING LEAD LOOP DESIGN

The basic design of the duct for the molten lead loop is relatively simple. A rectangular duct was chosen for two primary reasons. The first reason is that in the converter section of the loop, the flow must be narrowed to 0.25-cm thickness in the beam path. If a circular pipe or square duct had been used this would have resulted in a very large change of flow area, thereby causing a large pressure drop. With the rectangular duct there is still a significant change in flow area, but it is not as severe. The second reason is the use of an electromagnetic force pump. For electromagnetic force pumps to work efficiently the channel which they are used on must be significantly wider than it is tall. Therefore, either the entire duct must be rectangular or there must be a significant change in the channel dimensions in the region of the pump. The exact mechanics for these pumps are discussed further on. After considering these two factors, it was obvious that the most effective solution was to construct the entire loop out of a rectangular duct, rather than to have multiple circular-rectangle transition regions. A rectangular cross-section of 1-cm by 4-cm was chosen so as to allow the duct to be modeled as a normal internal flow system. Elongating the duct further would have unnecessarily complicated the heat transfer modeling without serving any real benefit to the heat transfer or pumping system.

The material chosen for the duct walls is type 314 stainless steel. Stainless steel is an obvious choice for molten metal system, due to its excellent resistance to corrosion by the liquid metal [1,9]. Stainless steel type 314 is composed of 53% iron, 25% chromium, 20.5% nickel, 1% manganese, 0.5% silicon, and <0.2% carbon by weight fraction. This is

an austenitic type stainless steel. An austenitic stainless steel was chosen because other types of stainless steel are ferromagnetic and could therefore interfere with the magnetic field lines in the electromotive force pump.

6.2 HEAT EXCHANGE SYSTEM

The heat exchange system to be used in conjunction with the molten lead loop offered an interesting design challenge. The lead flowing in the duct must be maintained at an average temperature well above its melting point of 600K to avoid problems with spot freezing along the heat exchanger walls. For a variety of structural and operational reasons it is desirable to use a heat exchanger with the coolant side using water flowing at room temperature, at low pressure, and with easily produced flow rates. Such a system is easy to construct and operate since there are none of the difficulties associated with high pressure. However, room temperature water has a tendency to flash boil, unless it is traveling at a very high flow rate, when it comes in contact with 600K surfaces. Flash boiling inside of the cooling ducts is unacceptable since it can create problems such as excessive corrosion, pressure pockets, and blowbacks. Therefore, either the channel wall temperature must be lowered or the pressure of the water increased.

Lowering the wall temperature for the water channel, while maintaining the high wall temperature for the lead channel, is actually quite simple. A buffer, of sorts, is placed between the lead and water channel. This buffer is simply a piece of metal thick enough to create the desired temperature gradient. This allows the lead channel wall to be maintained at well above lead's melting point, while the water channel wall is lowered to a more reasonable temperature for controlled heat transfer. The buffer will most likely be

constructed of a corrosion resistant steel, the reasoning for this is discussed further on. Figure 14 below shows a cross-section of the heat exchanger.

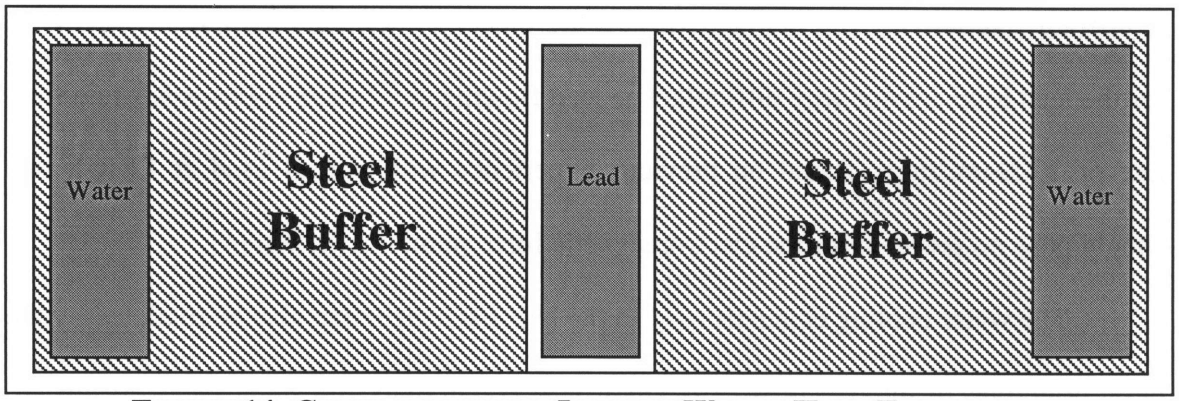

FIGURE 14: CROSS-SECTION OF LEAD TO WATER HEAT EXCHANGER

The modeling of the heat transfer process in the lead channel is a straightforward turbulent internal flow problem. The results from the optimum molten lead converter model show a heat deposition rate in the lead flow and surrounding stainless steel of 4,300 watts. Table XV below is the section of the spreadsheet model used to analyze the heat transfer from the lead flow to the channel walls.

TABLE XV: MODEL OF HEAT TRANSFER FROM LEAD TO CHANNEL WALL

Model of Heat Transfer in Lead Channel			
Length of Channel(cm):	20	Temp of SS at Tube:	658
Width of Channel(cm):	4	Surface area(cm^3):	160.00
Depth of Channel(cm):	1	Eq. Dia. of Tube(cm):	1.6
Density of lead(g/cm^3):	10.412	MFR lead(g/s):	500
Velocity of lead(cm/s):	12.00	Reynolds Number:	10384
Lead Viscosity(g/cm s):	0.0193	Nusselt Number:	6.6
Prandlt number:	0.017	HTC(w/cm^2K):	0.6404
Conductivity(w/cmK):	0.156	Total HT(w):	**4300**
Temperature of lead:	700		

The heat exchanger for the system is the 20-cm long section of the loop opposite the electromagnetic force pump. The 1-cm by 4-cm duct allows the principles of equivalent diameter to be used in the modeling process, making the analysis a relatively simple procedure. The stainless steel wall temperature is maintained at an average of 658K, a

full 60K above leads freezing point. The bulk change in temperature for the lead is about 60K for the total loop, therefore even at the end of the heat exchanger the wall temperature should not fall below 630K. As the model shows, the pumping requirements for the lead loop are not very difficult. The lead flowing at 12-cm/s corresponds to a flow rate of 2900-cm^3/min. Based on previous experience with pumps used at EBR-I, this should pose no problem for the electromagnetic force pumping system [4].

The water cooling channels used in the heat exchanger can also be modeled by the basic principles of internal flow. Like their lead counterpart, the water channels are 20-cm long and have a cross-section of 1-cm by 4-cm. However, there are two water channels, one on each side of the lead channel. A variety of other channel designs were considered, such as multiple small channels in both horizontal and vertical configurations, but none showed any significant advantage over the two-channel model. Table XVI below shows the analysis of the water channel.

TABLE XVI: MODEL OF HEAT TRANSFER FROM STEEL BUFFER TO WATER

Model of Water Cooling channels			
Width of Channel(cm):	1	Dia. of Channel(cm):	1.600
Height of Channel(cm):	4	Sur. area of tube(:cm^2)	160.0
Number of Channels:	2	Water Velocity(cm/s):	50.0
Length of Channel(cm):	20	Reynolds Number:	10403
MFR of Water(g/s):	200	Nusselt Number:	72.8
Temp of Water(K):	300	HTC(W/cm^2K):	0.282
Water Density(g/cm^3):	1.00	HT per tube(w):	2150
Water Viscosity(Ns/m^2):	7.69E-04	Total HT(w):	**4300**
Prandlt Number:	5.2	Rise in Bulk W Temp:	5.1
Cond. of Water(w/cmK):	0.0062	Temp of steel at chan. :	348
Specific heat water(j/gk):	4.184		

A fairly low channel wall temperature, 348K, was chosen to insure controlled heat transfer from the wall to the water flow, with little chance of complications such as flash boiling. For this configuration the system requires a mass flow rate of 200-g/s in each

flow channel, which corresponds to a total flow rate in the system of 24 liters per minute. This flow rate is easily achievable with a relatively small pump for the water.

The final step in the analysis of the heat exchanger is to examine the steel buffer between the lead channel and the water channels. This is a relatively straightforward heat conduction problem. The stainless steel wall, steel buffer, and the interface between the two must be accounted for in the model. Table XVII below shows the analysis of heat conduction through the buffer.

TABLE XVII: MODEL OF HEAT TRANSFER THROUGH THE STEEL BUFFER

Model of Iron Buffer Plate				
Temp. of SS at Tube:	658.0	Temp. of SS at Buffer:		619.6
Temp. of Iron at Channel:	347.7	Buffer Thickness(cm):		8.1
Thickness of SS(cm):	0.20			
Cond. of SS(w/cmK):	0.14			
Cond. of Iron(w/cmK):	0.8			

As the model shows, the required buffer thickness for the temperature drop of 310K is approximately 8-cm. Other materials, ranging from stainless steel to copper, were considered for the buffer. Steel was determined to be good selection based on its conductivity. Stainless steel's conductivity was too low, resulting in a buffer thickness of only 1.5-cm. Such a system would be more vulnerable to sudden operational changes. On the other hand, copper's conductivity is so high that the buffer would be 40-cm thick. Which is obviously unreasonable, though it would be a very stable system.

This is a accurate model of the heat exchanger designed for the molten lead converter, sufficient to demonstrate a broad design window. Through minor operational changes to the flow rates in the lead and water channels the system can be adjusted to remove the deposited heat while maintaining the lead above its freezing point and the water well below its boiling point.

6.3 ELECTROMAGNETIC FORCE PUMP

Electromagnetic force (EMF) pumps have been used for years in a variety of applications, including the Experimental Breeder Reactor (EBR-I) and in the circuit board industry for pumping solder. While they have been used for quite a while, they are typically built for specific situations. A preliminary search suggests that an EMF pump will have to be custom built for this application. The following is a discussion of the basic design issues behind an EMF pump and what the pumping requirements of this system will be.

The scientific theory behind an EMF pump is derived from the principles of electromagnetism [4]. By crossing magnetic field lines along the x-axis and electric current lines along the y-axis a driving force is created on the z-axis. The magnitude of this force, in Newtons, is given by

$$F = B \cdot I_e \cdot a$$

where B = Magnetic Field Flux (T)
I_e = Current (A)
a = Height of Duct (cm)

If the molten lead in the system loop is used as the conductor of electricity in the circuit described above then the created force acts upon the lead. Since the lead is a liquid, this force causes the lead to begin flowing in the indicated direction through the loop, thus creating a pump with absolutely no moving parts.

This type of system is relatively easy to design at the conceptual level. Copper conductors attached to the narrow sides of the stainless steel duct provide the current to the lead flow, while electromagnetic poles placed to the right and left of the duct supply

the magnetic field. Figure 15 below shows the current and field lines for this pump, with the lead flow coming directly out of the page.

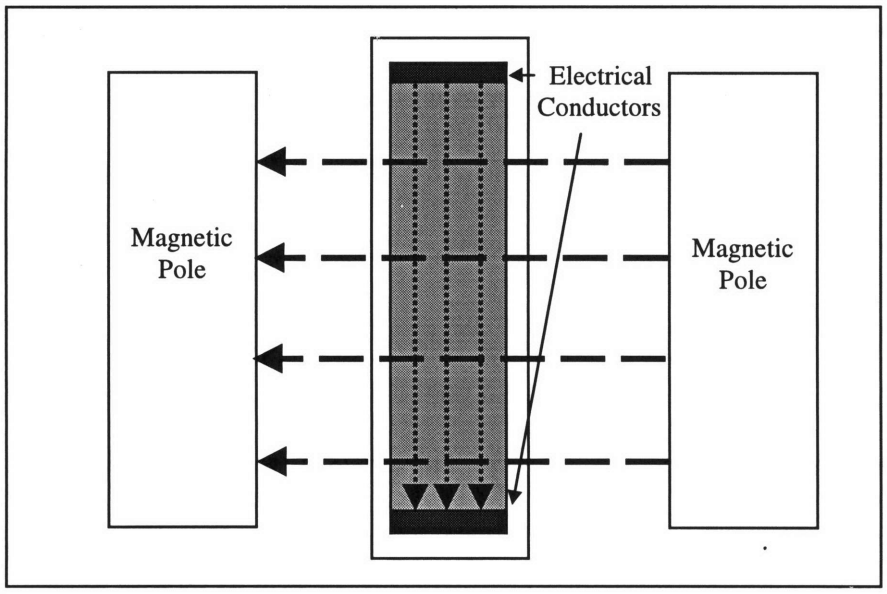

FIGURE 15: DIAGRAM OF ELECTROMAGNETIC FORCES IN EMF PUMP

Since pressure is simply force divided by area, the pressure rise created by this pump is given by

$$\Delta p = \frac{F}{A} = \frac{B \cdot I_e}{b}$$

where b = Width of Duct (cm)

Therefore, the current supplied to the pump is increased until the pressure rise generated in the pump balances the pressure loss in the rest of the loop. The current requirements for EMF pumps are quite high, for example, approximately 1,000 Amps would be required for a typical 20,000 cm^3/sec pumping system.

The difficulty in modeling these pumps is in solving the electrical circuit they form. There are three possible routes for the current to take in traveling from the top of the duct to bottom of the duct. The first and most obvious route is through the molten lead in the duct. This is the current that is useful for the pumping mechanism. However,

one complication of this is that it is possible for the current to flow through the lead, but outside of the magnetic field. This is the second route current can take and is useless to the pumping mechanism. The third possibility is for the current to enter the duct wall and not flow through the lead at all. This is also wasted current. To solve for the current used in the equations above, the electrical resistance of these three paths must be determined. The resistance through the lead flow is easy, it simply a mater of multiplying the height of the duct by the resistivity of lead. The resistances of the fringe and wall routes are not so easy. In fact, there is no current known method to solve for them directly, they have to be either experimentally or numerically determined. One thing is known though, the higher these resistances are the more current flows directly through the lead, increasing the pump's efficiency.

One method of increasing the resistance to fringe current is to add insulating vanes parallel to the flow just outside the entrance and exit of the pump. These vanes effectively reducing the distance outside of the magnetic field that the fringe current is allowed to flow. This same type of principle can be applied to reducing the current that flows through the walls of the duct. Coating or covering the right and left sides of the duct with an insulating material should significantly reduce the amount of current that flows through the walls. A high-temperature corrosion resistant ceramic, such as alumina (Al_2O_3), would be ideal for both of these situations. Alumina is commonly used as a crucible material for molten metals and in situations where a high strength ceramic is needed [1]. In fact, it may even be possible to form the entire duct in the pumping section of the loop out of alumina or another ceramic. This would effectively eliminate the wall flow current and, by the use of the vanes, severely reduce the fringe flow current.

6.4 Minor Subcomponents of Lead Loop

6.4.1 Startup Heating System

One of the main problems associated with a molten lead system is that at room temperature the lead is solid. Therefore, whenever the system is to be used the lead in the loop must first be melted in order for the pumping system to be able to function. Simply starting the beam is unacceptable since the area of the loop near the converter would become far too hot before the entire loop melted. Therefore, a system must be incorporated into the design that will allow the entire loop to be brought up to operational temperature without creating damaging hot spots.

The startup heating system is based on the use of simple resistive heating elements that have been attached directly to the stainless steel duct. Flexible heating elements, in the form of insulation wrapped tape, are commonly available through a variety of industrial sources. Many of these elements are able to reach temperatures in excess of 2000K under normal operation. Therefore by placing this tape along the entire length of the loop, it becomes a very simple matter to raise the temperature of the lead above its 600K melting point. The resistive tape will be place along the interior edge of the loop, except in the region of the pump. The pump region is excluded for two reasons. First, the operation of the pump is based on the electrical and magnetic field line present in the region, the tape could pose an interference with this and is therefore to be avoided. Second, the pump supplies a high current electrical circuit across the lead flow by itself. When the lead is solid, this electrical current will quickly raise its temperature above its melting point.

6.4.2 Level Control and System Monitoring

There should be minimal off gassing in the molten lead, however some small amount is almost always present in high temperature systems. Even a small amount of entrained gas in the lead flow will have an adverse reaction on the efficiency of the electromagnetic force pump. There would also be a reduction in molybdenum yield if the pockets of entrained gas were to pass through the beam spot of the converter region in the loop, though this effect would be minimal. Because of the issues with entrained gas and the electromagnetic force pump it is necessary to include some type of gas trap in the system design.

This task can be accomplished by placing a level control tank at the highest point in the lead loop. Since the current design of the loop doesn't have a singular highest point, the loop will be placed at a small angle making the region of the loop just before the pump the highest point. A 1-cm^2 hole is made in the top of the rectangular duct and small containment tank is attached. This tank will serve as not only an off gas collection tank, but also as a level control tank for the lead. By filling the tank to the halfway point it will provide not only a volume for any gas but also excess lead inventory.

During normal operations the rate at which the lead is flowing will not allow entrained gas to collect at the top of the flow. Therefore it will be necessary to periodically perform an off-gas collection operation. This would be performed by drastically decreasing the flow rate of the lead while maintaining operational temperature through the startup heating system. The lead flow would then be stopped so as to allow the gas to rise to the top of the channel and into the tank. After removing any initial impurities in the system, such a procedure would not need to be performed very often, if

at all. The level control tank also provides a convenient means of filling the system initially.

Both the lead and water temperatures of the system will need to be closely monitored to ensure efficient operation of the molten lead loop. Temperature sensors should be placed in the lead flow at the entrance and exit of both the pump and the heat exchanger. By placing the sensors at these four points an accurate assessment of the lead's minimum, maximum, and average temperatures can be made. Theoretically, the lead flow's maximum temperature should be at the heat exchanger entrance and the minimum at the pump entrance. The water temperature at both the entrance and exit of the heat exchanger should also be monitored. By monitoring these temperatures it will allow operators to adjust system flow parameters as needed. While a variety of other monitoring equipment will be need for this system, the temperature sensors are by far the most critical to the system.

7. CONCLUSIONS

This study has presented two alternative electron to photon converter designs for use in the production of ^{99m}Tc and other radioisotopes. The primary focus of the engineering for these designs was the maximization of the photoneutronic reaction rate in the ^{100}Mo target slug, thereby maximizing the specific activity of the isotope being produced. The simplicity and reliability of the systems was also of great importance. Many specific engineering issues were not addressed in this study and have been left for further investigations. These include target optimization, target cooling systems, magnetic sweep design, and radiation shielding. While these components are all important to a final system design, they are unlikely to effect the final design of the electron to photon converter.

The feasibility of a radiantly cooled target was explored during the first phase of the project. The optimized configuration of the radiantly cooled converter was determined to be a single inclined slab with a horizontal length of 5-cm and an equivalent thickness of .05-cm. This converter produced a yield of 4.914 ± 0.137 mb/cm^2 in the molybdenum target slug, while maintaining a maximum surface temperature for the tungsten of less than 3000K. While this is an 80% increase in yield over the baseline PMHX case, it is also the operational limit of the radiantly cooled design. The yield could not be increased by use of a larger electron accelerator because the heat transfer limits of the radiantly cooled design have been reached. Therefore, for a lower specific activity production system the radiantly cooled converter is ideal because of its reliability. A radiantly cooled converter has no moving parts and is therefore not prone to normal mechanical failures and maintenance outage.

In the second phase of the project a molten lead converter design was investigated for use in the production of ^{99m}Tc. This design was investigated because of its superior heat load handling characteristics. Because the system is circulating loop of molten metal, it is able to absorb and dissipate a great deal more energy than its radiantly cooled counterpart. An optimized design, composed of a lead converter region 0.25-cm thick and a electron beam energy of 40-MeV, was capable of producing a yield of 8.457±0.023 mb/cm^2 in the molybdenum target, a 309% increase over the PMHX tungsten slug. A basic design of a heat exchanger for the molten lead flow was also presented. An electromagnetic force pump was chosen to provide pumping power for this system to eliminate moving parts in the coolant loop. Heat transfer is provided by a thick-walled counter flow heat exchanger. This system is capable of removing the heat deposited in the lead while operating at very easily achievable system flow parameters. The heat exchanger can easily be modified to handle a much higher energy deposition rate than presented here. In fact, the only limiting factor of the heat rejection system is the specific energy deposition in the stainless steel duct surrounding the lead flow in the region of the electron beam. The current system, based on a LINAC designed by Titan Beta, is limited by the output of the accelerator. This system could easily be re-engineered to take advantage of a larger electron accelerator.

The feasibility of these alternative electron to photon converter designs has been demonstrated and the system parameters presented for all systems are well within allowable engineering limits. The molten lead converter is capable of producing an increased flux of GDR photons on target and is therefore capable of substantially improving the capacity of a radioisotope production facility.

APPENDIX A

MODEL 1: PHMX SLUG

```
TEST MODEL 1:  BASIC MODEL OF ELECTRON BEAM STRIKING A SLUG TARGET
1     1  -11.58  -1  2 -3      $ TUNGSTEN SLUG
2     0          -2 -6         $ VOID SPACE BEFORE TARGET
3     0           1  2 -3 -6   $ VOID AROUND THE TARGET
4     0           3 -4 -6      $ VOID BETWEEN T AND D
5     2  -10.2    4 -5 -1      $ MOLYBDENUM SLUG
6     0           4 -5  1 -6   $ VOID AROUND THE DETECTOR
7     0           5 -6         $ VOID AFTER DETECTOR
8     0           6 -7         $ VOID OF OUTER SPHERE
9     0           7            $ REST OF WORLD

1     CX  0.500   $  CYLINDER DEFINING TARGET
2     PX  0.000   $  PLANE DEFINING START OF TARGET
3     PX  0.583   $  PLANE DEFINING END OF TARGET
4     PX  5.583   $  PLANE FOR START OF DETECTOR
5     PX  6.583   $  PLANE FOR END OF DETECTOR
6     SO 15.000   $
7     SO 16.000   $

SDEF  ERG=40   DIR=1 VEC=1 0 0 POS=-10 0 0 RAD=D1 AXS=1 0 0 PAR=3
SI1    0.5
PRDMP  50000 -1 0 5 0
IMP:P 1 1 1 1 1 1 1 0
IMP:E 1 1 1 0 1 1 1 0
MODE  P E
M1 74000 1
M2 42100 1
NPS 500000
CUT:P J 0.5
CUT:E J 0.5
C TALLY NUMBER 4: MOLY PRODUCTION TALLY
F4:P 5
E4 8 23I 20 T
EM4 0 2 11 12 16 18 33 52 71 87 108 130 146 132 110 87 65 48 46 37 22 &
    12 6 2 0
FQ4 E S
C TALLY NUMBER 21: ELECTRONS AFTER CONVERTER
*F21:E 3
FS21 -6 T
FQ21 E S
C TALLY NUMBER 8: ENERGY ABSORBED IN CONVERTER
*F8:P,E 1
C TALLY NUMBER 18: ENERGY ABSORBED IN TARGET
*F18:P,E 5
C TALLY OF ELECTRONS ESCAPING SYSTEM
*F31:E 6
FS31 -3 T
FQ31 E S
C TALLY OF PHOTONS ESCAPING SYSTEM
*F41:P 6
```

MODEL 2: SINGLE INCLINED PLANE

```
TEST MODEL 2:  BASIC MODEL OF ELECTRON BEAM STRIKING INCLINED SLAB
1     1  -19.30  1 -2  3  -4 5 -6  IMP:P,E=1 $ TUNGSTEN SLAB
2     0          -3 -9             IMP:P,E=1 $ VOID SPACE BEFORE TARGET
3     0           3 -4 -5  -11     IMP:P,E=1 $ VOID TO LEFT OF TARGET
4     0           3 -4  6  -11     IMP:P,E=1 $ VOID TO RIGHT OF TARGET
5     0          -1  3 -4 5 -6 -11 IMP:P,E=1 $ VOID ABOVE THE TARGET
6     0           2  3 -4 5 -6 -11 IMP:P,E=1 $ VOID BELOW THE TARGET
7     0           3 -4  11 -9      IMP:P,E=1 $ VOID AROUND TARGET ASSEM
8     0           4 -7 -9          IMP:P=1 IMP:E=0 $ VOID CON AND SLUG
9     2  -10.2    7 -8 -12         IMP:P,E=1   $ MOLY SLUG
10    0           7 -8 12  -9      IMP:P,E=1 $ VOID AROUND SLUG
11    0           8 -9             IMP:P,E=1 $ VOID AFTER SLUG
12    0           9 -10            IMP:P,E=1 $ VOID OF OUTER SPHERE
13    0           10               IMP:P,E=0 $ REST OF WORLD

1     P   0.2 0.0 -1 0.500  $ TOP PLANE OF TARGET
2     P   0.2 0.0 -1 0.510  $ BOTTOM PLANE
3     PX  0.000   $  PLANE DEFINING START OF TARGET
4     PX  5.100   $  PLANE DEFINING END OF TARGET
5     PY -0.600   $  PLANE FOR LEFT SIDE OF TARGET
6     PY  0.600   $  PLANE FOR RIGHT SIDE OF TARGET
7     PX 10.100   $  PLANE FOR START OF MOLY SLUG
8     PX 11.100   $  PLANE FOR END OF MOLY SLUG
9     SO 59.000   $
10    SO 60.000   $
11    CX  1.000   $
12    CX  0.50

SDEF  ERG=40   DIR=1 VEC=1 0 0 POS=-10 0 0 RAD=D1 AXS=1 0 0 PAR=3
SI1    0.5
PRDMP 250000 -1 0 5 0
MODE  P E
M1 74000 1
M2 42100 1
NPS 25000
ELPT:P 0.5
ELPT:E 0.5
C TALLY NUMBER 4: MOLY PRODUCTION TALLY
F4:P 9
E4 8 23I 20 T
EM4 0 2 11 12 16 18 33 52 71 87 108 130 146 132 110 87 65 48 46 37 22 &
    12 6 2 0
FQ4 E S
C TALLY NUMBER 8: ENERGY ABSORBED IN CONVERTER
*F8:P,E 1
C TALLY NUMBER 18: ENERGY ABSORBED IN TARGET
*F18:P,E 9
C TALLY OF ELECTRONS ESCAPING SYSTEM
*F31:E 9
C TALLY OF PHOTONS ESCAPING SYSTEM
*F41:P 9
```

MODEL 3: MULTIPLE INCLINED PLANES

```
TEST MODEL 1:  BASIC MODEL OF ELECTRON BEAM STRIKING MULTIPLE PLANE TARGETS
1     1  -19.30  1 -2  3 -15 5 -6 IMP:P,E=1 $ TUNGSTEN SLAB1
2     1  -19.30 -13 14 15 -4 5 -6 IMP:P,E=1 $ TUNGSTEN SLAB2
3     0         -3 -9             IMP:P,E=1 $ VOID SPACE BEFORE TARGET
4     0          3 -15 -5  -11    IMP:P,E=1 $ VOID TO LEFT OF TARGET1
5     0          3 -15  6  -11    IMP:P,E=1 $ VOID TO RIGHT OF TARGET1
6     0         -1 3 -15 5 -6 -11 IMP:P,E=1 $ VOID ABOVE THE TARGET1
7     0          2 3 -15 5 -6 -11 IMP:P,E=1 $ VOID BELOW THE TARGET1
8     0          15 -4 -5 -11     IMP:P,E=1 $ VOID TO LEFT OF T2
9     0          15 -4  6 -11     IMP:P,E=1 $ VOID TO RIGHT OF T2
10    0         13 15 -4 5 -6 -11 IMP:P,E=1 $ VOID ABOVE T2
11    0        -14 15 -4 5 -6 -11 IMP:P,E=1 $ VOID BELOW T2
12    0           3 -4  11 -9     IMP:P,E=1 $ VOID AROUND TARGET ASSEM
13    0           4 -7 -9         IMP:P,E=1 $ VOID BETWEEN CON AND SLUG
14    2  -10.2    7 -8 -12        IMP:P=1 IMP:E=0 $ MOLY SLUG
15    0           7 -8 12  -9     IMP:P,E=1 $ VOID AROUND SLUG
16    0           8 -9            IMP:P,E=1 $ VOID AFTER SLUG
17    0           9 -10           IMP:P,E=1 $ VOID OF OUTER SPHERE
18    0           10              IMP:P,E=0 $ REST OF WORLD

1     P   0.40404 0.0 -1 0.5000  $ TOP PLANE OF TARGET
2     P   0.40404 0.0 -1 0.5101  $ BOTTOM PLANE
3     PX  0.000   $  PLANE DEFINING START OF TARGET
4     PX  5.000   $  PLANE DEFINING END OF TARGET
5     PY -0.600   $  PLANE FOR LEFT SIDE OF TARGET
6     PY  0.600   $  PLANE FOR RIGHT SIDE OF TARGET
7     PX 10.350   $  PLANE FOR START OF MOLY SLUG
8     PX 11.350   $  PLANE FOR END OF MOLY SLUG
9     SO 59.000   $
10    SO 60.000   $
11    CX  1.000   $
12    CX  0.50
13    P -0.40404 0.0 -1 -1.5101 $ PLANE DEFINING BOTTOM OF SECOND
14    P -0.40404 0.0 -1 -1.5202 $ PLANE DEFINING TOP OF SECOND
15    PX 2.500  $ PLANE DEFINING CONVERTER SEPERATION
16    PZ -1.00
17    PZ -0.75
18    PZ -0.50
19    PZ -0.25
20    PZ  0.00
21    PZ  0.25
22    PZ  0.50
23    PZ  0.75
24    PZ  1.00

SDEF  ERG=40   DIR=1 VEC=1 0 0 POS=-10 0 0 RAD=D1 AXS=1 0 0 PAR=3
SI1    0.5
MODE  P E
M1 74000 1
M2 42100 1
NPS 50000
CUT:P J 4.0
CUT:E J 4.0
C TALLY NUMBER 4: MOLY PRODUCTION TALLY
F4:P 14
E4 8 23I 20 T
EM4 0 2 11 12 16 18 33 52 71 87 108 130 146 132 110 87 65 48 46 37 22 &
    12 6 2 0
FQ4 E S
C TALLY NUMBER 8: ENERGY ABSORBED IN CONVERTER
*F8:P,E 1 2
C TALLY NUMBER 18: ENERGY ABSORBED IN TARGET
*F18:P,E 14
C TALLY OF ELECTRONS ESCAPING SYSTEM
*F31:E 9
C TALLY OF PHOTONS ESCAPING SYSTEM
*F41:P 9
```

MODEL 4: CONE MODEL

```
CONE MODEL
1     1  -19.30   -1  2  3 -4    IMP:P,E=1 $ TUNGSTEN CONE
2     1  -19.30   -1  4 -5       IMP:P,E=1 $ TUNGSTEN CONE TIP
3     0           -3 -7          IMP:P,E=1 $ VOID BEFORE TARGET
4     0            3 -4  1 -7    IMP:P,E=1 $ VOID AROUND TARGET
5     0           -2  3 -4       IMP:P,E=1 $ VOID INSIDE TARGET
6     0            4 -5  1 -7    IMP:P,E=1 $ VOID AROUND TIP
7     0            5 -6 -7       IMP:P,E=1 $ VOID BETWEEN T AND D
8     2  -10.2     6 -10 -9      IMP:P=1 IMP:E=0 $ MOLY SLUG
9     0            6 -10 9 -7    IMP:P,E=1 $ VOID AROUND SLUG
10    0            10 -7         IMP:P,E=1 $ VOID AFTER DETECTOR
11    0            7 -8          IMP:P,E=1 $ VOID BETWEEN SPHERES
12    0            8             IMP:P,E=0 $ REST OF WORLD

1   KX 10.0 .00255076
2   KX  9.9 .00255076
3   PX 0
4   PX  9.9
5   PX 10.0
6   PX 13.0
7   SO 20
8   SO 21
C THE REST OF THE SURFACES ARE FOR TALLIES
9   CX 0.5
10  PX 14

SDEF  ERG=40   DIR=1 VEC=1 0 0 POS=-10 0 0 RAD=D1 AXS=1 0 0 PAR=3
SI1    0.5
MODE  P E
M1 74000 1
M2 42000 1
NPS 20000
CUT:P J 0.5
CUT:E J 0.5
C TALLY NUMBER 4: PHOTONS AFTER TARGET
F4:P 8
E4 8 23I 20 T
EM4 0 2 11 12 16 18 33 52 71 87 108 130 146 132 110 87 65 48 46 37 22 &
    12 6 2 0
FQ4 E S
C TALLY NUMBER 8: ENERGY ABSORBED IN TARGET
*F28:P,E 1
E28 5 10 15 20
*F38:P,E 2
C TALLY OF ELECTRONS ESCAPING SYSTEM
F31:E 7
C TALLY OF PHOTONS ESCAPING SYSTEM
F41:P 7
```

MODEL 5: MOLTEN LEAD FLOW MODEL

```
TEST MODEL 1:  BASIC MODEL OF ELECTRON BEAM STRIKING A SLUG TARGET
1   1  -11.4  2 -3  6 -7 -11   IMP:P,E=1  $ LEAD CONVERTER
2   2  -8.0   1 -2  5 -8 -11   IMP:P,E=1  $ SS HOUSING
3   2  -8.0   3 -4  5 -8 -11   IMP:P,E=1  $ SS HOUSING
4   2  -8.0   2 -3  5 -6 -11   IMP:P,E=1  $ SS HOUSING
5   2  -8.0   2 -3  7 -8 -11   IMP:P,E=1  $ SS HOUSING
6   0        -1 -11            IMP:P,E=1  $ VOID BEFORE CONVERTER
7   0         1 -4 -5 -11      IMP:P,E=1  $ VOID TO LEFT OF CONVERTER
8   0         1 -4  8 -11      IMP:P,E=1  $ VOID TO RIGHT OF CONVERTER
9   0         4 -9 -11         IMP:P,E=1  $ VOID BETWEEN CON AND MOLY
10  3  -10.2  -13 9 -10        IMP:P=1 IMP:E=0 $ MOLY SLUG
11  0         13 9 -10 -11     IMP:P,E=1  $ VOID AROUND MOLY SLUG
12  0         10 -11           IMP:P,E=1  $ VOID AFTER MOLY SLUG
13  0         11 -12           IMP:P,E=1
14  0         12               IMP:P,E=0

1  PX   -0.300 $ OUTER PLANE OF FRONT CHANNEL
2  PX   -0.250 $ INNER PLANE OF FRONT CHANNEL
3  PX   -0.000 $ INNER PLANE OF BACK CHANNEL
4  PX    0.050 $ OUTER PLANE OF BACK CHANNEL
5  PY   -0.550 $ OUTER PLANE OF LEFT CHANNEL
6  PY   -0.500 $ INNER PLANE OF LEFT CHANNEL
7  PY    0.500 $ INNER PLANE OF RIGHT CHANNEL
8  PY    0.550 $ OUTER PLANE OF RIGHT CHANNEL
9  PX    5.000 $ FRONT PLANE OF MOLY SLUG
10 PX    6.000 $ BACK PLANE OF MOLY SLUG
11 SO   30.000
12 SO   31.000
C  REST USED FOR TALLY ONLY
13 CX    0.500

SDEF  ERG=40   DIR=1 VEC=1 0 0 POS=-10 0 0 RAD=D1 AXS=1 0 0 PAR=3
SI1    0.5
MODE  P E
M1 82000 1
M2 26000 -0.530 14000 -0.005 25055 -0.010 28000 -0.205 24000 -0.250
M3 42000 1
NPS 500000
CUT:P J 1.0
CUT:E J 1.0
C TALLY NUMBER 4: PHOTONS AFTER TARGET
F4:P 10
E4 8 23I 20 T
EM4 0 2 11 12 16 18 33 52 71 87 108 130 146 132 110 87 65 48 46 37 22 &
    12 6 2 0
FQ4 E S
C TALLY NUMBER 8: ENERGY ABSORBED IN TARGET
*F8:P,E 1 10 2 3 4 5
C TALLY OF ELECTRONS ESCAPING SYSTEM
*F31:E 11
C TALLY OF PHOTONS ESCAPING SYSTEM
*F41:P 11
```

APPENDIX B

Controllable Variables:	
Beam Diameter(cm):	1
Needed Equiv. Length(cm):	0.0501
Angle of Incidence:	11.3107
Time Step(sec):	0.0002
Boltzmann(w/cm2k4):	5.67E-12
Density(g/cm3):	19.3
Emissivity:	0.275
Surface Temp(K):	300
Number of Plates:	1
System Power(watts):	935

Calculated Variables:	
Delta X(cm):	0.0579
Delta Y(cm):	0.0278
Delta Z(cm):	0.0098061
Target Length(cm):	5.00
Power For Cell(watts):	0.3752

LEAD FLOW MODEL

Model of Water Cooling channels				
Width of Channel(cm):	1	Dia. of Channel(cm):		1.600
Height of Channel(cm):	4	Sur. area of tube(:cm^2)		160.0
Number of Channels:	2	Water Velocity(cm/s):		50.0
Length of Channel(cm):	20	Reynolds Number:		10403
MFR of Water(g/s):	200	Nusselt Number:		72.8
Temp of Water(K):	300	HTC(W/cm^2K):		0.282
Water Density(g/cm^3):	1.00	HT per tube(w):		2150
Water Viscosity(Ns/m^2):	7.69E-04	Total HT(w):		**4300**
Prandlt Number:	5.2	Rise in Bulk W Temp:		5.1
Cond. of Water(w/cmK):	0.0062	Temp of steel at chan. :		348
Specific heat water(j/gk):	4.184			

Model of Heat Transfer in Lead Channel				
Length of Channel(cm):	20	Temp of SS at Tube:		658
Width of Channel(cm):	4	Surface area(cm^3):		160.00
Depth of Channel(cm):	1	Eq. Dia. of Tube(cm):		1.6
Density of lead(g/cm^3):	10.412	MFR lead(g/s):		500
Velocity of lead(cm/s):	12.00	Reynolds Number:		10384
Lead Viscosity(g/cm s):	0.0193	Nusselt Number:		6.6
Prandlt number:	0.017	HTC(w/cm^2K):		0.6404
Conductivity(w/cmK):	0.156	Total HT(w):		**4300**
Temperature of lead:	700			

Model of Iron Buffer Plate				
Temp. of SS at Tube:	658.0	Temp. of SS at Buffer:		619.6
Temp. of Iron at Channel:	348	Buffer Thickness(cm):		8.1
Thickness of SS(cm):	0.20			
Cond. of SS(w/cmK):	0.14			
Cond. of Iron(w/cmK):	0.8			

REFERENCES

1. Askeland, Donald R., 1989, The Science and Engineering of Materials, PWS-Kent Publishing Company, Boston, MA.

2. Briesmeister, Judith F., ed., 1993, MCNP-A General Monte Carlo N-Particle Transport Code, Version 4A, RSIC.

3. Cabbage, Bill, January 1995, "The Radioisotope Crunch," Oak Ridge National Laboratory Labnotes.

4. El-Wakil, M. M., 1993, Nuclear Heat Transport, The American Nuclear Society, La Grange Park, IL.

5. Incropera, F.P. and DeWitt, D.P., 1990, Introduction to Heat Transfer, John Wiley & Sons, Inc., New York, NY.

6. Krane, Kenneth S., 1988, Introductory Nuclear Physics, John Wiley & Sons, Inc., New York, NY.

7. Lamarsh, John R., 1983, Introduction to Nuclear Engineering, Addison-Wesley Publishing Company, Inc., Reading, MA.

8. Lidsky, L.M., March 27, 1995, *Research Program Prospectus*, presented to The INEL University Research Consortium.

9. Ma, Benjamin M., 1983, Nuclear Reactor Materials and Applications, Van Nostrand Reinhold Company, New York, NY.

10. Tune, Lee, December 14, 1994, " U.S. Should Take steps to Keep Supply of Medical Isotopes Adequate", Institute of Medicine News, National Academy of Sciences.